A quasinormal scale elimination model of turbulent flows with stable stratification

Semion Sukoriansky[a)]
Department of Mechanical Engineering/Perlstone Center for Aeronautical Engineering Studies, Ben-Gurion University of the Negev, Beer-Sheva 84105, Israel

Boris Galperin
College of Marine Science, University of South Florida, Saint Petersburg, Florida 33701

Ilya Staroselsky
EXA Corporation, Burlington, Massachusetts 01803

(Received 13 January 2005; accepted 5 July 2005; published online 23 August 2005)

A new spectral model for turbulent flows with stable stratification is presented. The model is based on a quasi-Gaussian mapping of the velocity and temperature fields using the Langevin equations and employs a recursive procedure of small-scale mode elimination that results in a coupled system of differential equations for effective, horizontal and vertical, viscosities and diffusivities. With increasing stratification, the vertical viscosity and diffusivity are suppressed while their horizontal counterparts are enhanced thus explicitly accounting for the anisotropy introduced by stable stratification. The new model is used to derive various spectral characteristics of stably stratified turbulent flows. It accounts for energy accumulation in the horizontal components at the expense of the energy reduction in the vertical component. The scale elimination algorithm explicitly accounts for the combined effect of turbulence and internal waves. A modified dispersion relation for internal waves, a relationship for internal wave frequency shift, and a threshold criterion for internal wave generation in the presence of turbulent scrambling are derived. It is shown how the model can be utilized to derive parameters needed for Reynolds-averaged Navier-Stokes modeling. Implemented in the K-ϵ format, the new model produces results that agree very well with the observational data on stably stratified atmospheric boundary layers and that are difficult to obtain using traditional two-equation turbulence modeling. © *2005 American Institute of Physics*.
[DOI: 10.1063/1.2009010]

I. INTRODUCTION

Turbulent flows with stable stratification are common in nature. Circulations of planetary and terrestrial atmospheres, oceans, and lakes are all examples of such flows. In a stably stratified environment, the gravity force leads to existence of internal gravity waves, and, in addition, to anisotropization of the dynamical and transport properties of the flow field. Understanding and predicting of such flows are of considerable theoretical and practical importance; extensive research has yielded a large volume of experimental, observational, descriptive, heuristic, and computational information over the years. To characterize different flow regimes emerging in stably stratified flows, numerous spatial and temporal scales and nondimensional parameters have been introduced and various heuristic, semiempirical, and analytical theories have been developed.[1–13] However, present understanding of stably stratified turbulence is far from complete. The characterization of data collected in various flow regimes often appears inconsistent and confusing reflecting the diversity of the environmental conditions (laboratory facilities, atmospheric boundary layers, oceanic mixed layers, lakes, stratosphere and troposphere, low Reynolds number computer simulations, etc.). There exists an unfortunate disconnect between models and approaches used in different fields, such as analytical theories, boundary layer meteorology, high-altitude meteorology, and physical oceanography. In this paper, we attempt to construct a theory of stably stratified turbulence which is reasonably proximate to the first principles and at the same time leads to predictions that can be directly used in these diverse practical applications.

Technically speaking, one of the central problems of analytical theories of turbulence is the treatment of nonlinear terms in the governing equations. Within the conventional, perturbative nonlinearity treatment, a straightforward scaling analysis suggests that a proper expansion parameter should be the Reynolds number Re that measures the ratio of the nonlinear and viscous terms. Notoriously, Re based upon the molecular viscosity and characteristic velocity and length scales of large energy containing eddies is very large and the corresponding expansion in powers of Re is strongly divergent. A class of analytical theories of turbulence exploits an expansion in powers of the *effective* Reynolds number built upon the effective, rather than molecular, viscosity.[14,15] Theories that employ such expansions have been coined *renormalized perturbation theories*, or RPT.[15] One of the important vehicles of RPT is the Langevin equation that arises in the lowest perturbative order. In the case of neutral stratification, the Langevin equation is

[a)]Electronic mail: semion@bgu.ac.il

$$u_i(\omega,\mathbf{k}) = G(\omega,\mathbf{k}) f_i(\omega,\mathbf{k}), \tag{1}$$

where ω and $\mathbf{k}$ are the Fourier frequency and wave number, $G(\omega,\mathbf{k})$ is the Green function, and $f_i(\omega,\mathbf{k})$ is a random force stirring the mode u_i. Physically, this modal forcing is the result of excitation of a given mode by all other modes due to nonlinear interactions. It is not related directly to the large-scale forcing that drives the system; instead, it quantifies the effect of this forcing upon the mode u_i transmitted by interaction of all other modes. The Green function, on the other hand, includes the effective viscosity and describes the damping of the mode $u_i(\omega,\mathbf{k})$ by nonlinear interaction with all other modes. Heuristically, in terms of the Kolmogorov cascade, the Langevin equation provides twofold characterization of the nonlinear interactions: the damping term in the Green function represents the energy transfer from a mode with a wave number k to higher wave-number modes whereas the random forcing $f_i(\omega,\mathbf{k})$ accounts for the energy transfer to the given mode from lower wave-number modes.

While the effective viscosity can be evaluated within RPT, the forcing $f_i(\omega,\mathbf{k})$ has defeated all attempts of theoretical derivation so far. In this paper, we postulate that, based upon transparent physical reasoning, the modal forcing should be taken as Gaussian and the amplitude of its correlation function is proportional to the rate of the large-scale energy input. The latter assumption enforces correct energy balance between forcing and damping of every Fourier mode at all times. In other words, the Langevin equations provide a device that facilitates the replacement of the original nonlinear Navier-Stokes equation by a system of linear, forced, stochastic equations in which the energy budget is systematically adjusted for every Fourier mode.[16] The replacement of the fully nonlinear Navier-Stokes equations by the Langevin equations can be viewed as a *mapping* of the original flow field onto a quasi-Gaussian field under the constraints of incompressibility and conservation of the modal energy flux.

The theory presented below in this paper belongs in the RPT family. It seeks to establish a self-consistent coarse-graining procedure yielding the effective viscosity and diffusivity for a stably stratified turbulent flow field. This procedure utilizes the key fact that for the modes adjacent to the dissipation range, Re is $O(1)$. Using the Langevin equation (1), small shells of the velocity and temperature modes can be ensemble averaged and excluded from the governing equations. The shell elimination procedure generates small corrections to the viscosity and diffusivity that account for the transport processes taking place on the eliminated scales. As a result, the effective dissipation wave number Λ decreases while the effective viscosity and diffusivity increase. The effective Re built upon the scales pertinent to the new value of Λ is again $O(1)$ such that the procedure can be repeated and another small shell of modes can be eliminated leading to further decrease of Λ and increase of the effective viscosity and diffusivity. This process can be continued until any predetermined wave number Λ is attained. The effective, Λ-dependent viscosities and diffusivities generated in this process can be related to subgrid scale (SGS) viscosities and diffusivities in large eddy simulations (LES) in which Λ is proportional to the inverse grid resolution.

Summarizing, let us highlight the four features of the present approach: (i) the theory aims at achieving a coarse-grained description of stably stratified turbulent flow field via successive elimination of small shells of modes in the vicinity of the dynamic dissipation cutoff wave number Λ where Re is $O(1)$; (ii) the Langevin equation is invoked for the modes designated for elimination; (iii) the forcing in the Langevin equation is postulated to be Gaussian and its amplitude is related to the rate of energy transfer through the given mode; and (iv) the modes are eliminated via ensemble-averaging whose by-products are the decrease of Λ (i.e., the incremental coarse graining of the system) and the increase of the effective viscosity and diffusivity. The assumptions involved in (iii) are critical because they lay the mathematical foundation sufficient for the development of a self-consistent model.

It is understood that the hypothesis of the Gaussianity is an approximation that, at best, yields good results for the second-order statistical moments. The deviations from Gaussianity affect higher-order moments. Since the effective viscosity and diffusivity are in the main focus of the present theory, the Gaussianity assumption is expected to yield reasonably accurate results.

The recursive procedure of small-scale elimination was formally introduced in Ref. 17 for systems with small expansion parameter. Later, it was applied to fluid turbulence in the framework of the renormalization group (RG) theory by Yakhot and Orszag (YO).[18,19] One of the important achievements of the YO theory of turbulence was establishing of the relationship between the amplitude of the modal forcing $f_\alpha(\omega,\mathbf{k})$ and an observable parameter, the rate of the energy injection on the large scales (equal to the rate of the viscous dissipation in steady state). The YO results were shown to be in good agreement with basic experimental, observational, and numerical data for neutrally stratified turbulence.[18,19] Another attractive feature of the YO theory is that it translates into transparent methodology using which the analytical results can be implemented in models designed for practically important applications, such as the K-ϵ models.[19] It needs to be mentioned that the original YO theory had several problematic foundational issues widely discussed in the literature. Some of these issues were clarified in Ref. 20 without affecting the results of the YO theory. Due to the advantages of this theory, the approach based upon the Gaussian approximation for the modal forcing and the procedure of recursive scale elimination has been adopted in the present study. Note, however, that there exist fundamental differences between the present and YO theories. The most critical distinction is that the former is not a RG theory in the theoretical physics understanding, i.e., it does not involve the rescaling and fixed-point arguments, and the modal forcing is not derived from the first principles. Instead, the scale invariance is not implied and the properties of the modal forcing are postulated. In this sense, the present theory is nothing else but a quasi-Gaussian spectral closure model of the RPT family. To reflect its main features, this model will be referred to as a quasinormal scale elimination (QNSE) model. By virtue of utilizing effective viscosity in modal equations, QNSE is an eddy-damped model.[14] The main difference that

sets the QNSE apart from other quasinormal models [such as eddy-damped, quasinormal Markovian (EDQNM),[14,21] EDQNM2,[4,22,23] EDQNM3,[24] etc.] is that the former employs a self-contained algorithm of successive small-scale mode elimination while the latter operate with complicated integrodifferential equations that involve all modes. As a result, the QNSE model is more amenable to analytical treatment than other models, particularly in flows with strong anisotropy and waves (note, however, that EDQNM2 and EDQNM3 do include anisotropy and waves).

The aforementioned simplicity of the QNSE model makes it possible to obtain insightful analytical results. For instance, a systematic process of small-scale elimination for stably stratified flow leads to the emergence of vertical and horizontal eddy viscosities and diffusivities thus reflecting the anisotropy introduced by stable stratification. Those eddy viscosities and diffusivities as well as various one-dimensional spectra can be calculated analytically in the case of weak stratification. The method also yields the dispersion relation for internal waves in the presence of turbulence and allows one to explore wave contribution to turbulence characteristics. The analysis reveals that at large wave numbers, turbulent scrambling overwhelms internal wave generation leading to the suppression of the wave regime. A corresponding spectral threshold criterion of internal wave generation in the presence of turbulence will be derived in Sec. X.

The paper is organized in the following fashion. Section II provides the outline of the basic assumptions and methods of the QNSE model. The relation between the Navier-Stokes and the Langevin equations underlying the idea of the quasi-Gaussian mapping is explained. Then we use successive small-scale mode elimination to derive two main equations that will eventually yield expressions for the effective viscosities and diffusivities defined in Sec. III. Sections IV and V provide detailed calculation of these effective viscosities and diffusivities while Sec. VI analyzes their behavior in the asymptotic case of weak stable stratification. In Sec. VII, a relationship between the forcing amplitude and the rate of the viscous dissipation ϵ is derived. This relationship allows one to express the effective turbulent transport coefficients in terms of the observable parameter ϵ. In Sec. VIII, the effective viscosities and diffusivities are characterized in terms of the Ozmidov wave number. Sections IX and X deal with the dispersion relation for internal waves in the presence of turbulence, turbulence-induced internal wave frequency shift, and the criterion of internal wave generation in the presence of turbulence. Section XI discusses various spectral characteristics of stably stratified turbulence. Section XII seeks to validate the theoretical derivations via comparisons with direct numerical simulations (DNS), laboratory, and field data and then to provide further validation of the QNSE model by implementing it in the K-ϵ format and applying the emerging K-ϵ model to simulate stably stratified atmospheric boundary layers. Finally, Sec. XIII provides discussion and conclusions.

II. MODEL OUTLINE

Consider fully three-dimensional, incompressible turbulent flow with externally imposed, homogeneous, stabilizing vertical gradient of the mean potential temperature Θ. The flow occupies an infinite domain and is governed by a system of the momentum (Navier-Stokes), temperature, and continuity equations in the Boussinesq approximation,

$$\frac{\partial \mathbf{u}}{\partial t} + (\mathbf{u}\cdot\nabla)\mathbf{u} - \alpha g T \hat{e}_3 = \nu_0 \nabla^2 \mathbf{u} - \frac{1}{\rho}\nabla P + \mathbf{f}^0, \tag{2}$$

$$\frac{\partial T}{\partial t} + (\mathbf{u}\cdot\nabla)T + \frac{d\Theta}{dz}u_3 = \kappa_0 \nabla^2 T, \tag{3}$$

$$\nabla\cdot\mathbf{u} = 0. \tag{4}$$

Here, P is the pressure, ρ is the constant reference density, ν_0 and κ_0 are the molecular viscosity and diffusivity, respectively, α is the thermal-expansion coefficient, g is the acceleration due to gravity directed downwards, and T is the fluctuation of Θ. The external solenoidal force $\mathbf{f^0}$ mimics the effect of large-scale instabilities and maintains turbulence in a statistically steady state. Note that the temperature equation (3) does not involve a separate forcing implying that the temperature fluctuations are excited by the velocity fluctuations. In the spectral domain bounded by the viscous dissipation (or Kolmogorov) wave number $k_d=(\epsilon/\nu_0^3)^{1/4}$ (ϵ is the rate of the viscous dissipation; $k_d\to\infty$ in the limit of an infinite Reynolds number), space-time Fourier transforms of the velocity and temperature fields are

$$u_i(\mathbf{x},t) = \frac{1}{(2\pi)^4}\int_{k\leqslant k_d} d\mathbf{k}\int d\omega u_i(\omega,\mathbf{k})\exp[i(\mathbf{kx}-\omega t)], \tag{5}$$

$$T(\mathbf{x},t) = \frac{1}{(2\pi)^4}\int_{k\leqslant k_d} d\mathbf{k}\int d\omega T(\omega,\mathbf{k})\exp[i(\mathbf{kx}-\omega t)]. \tag{6}$$

This yields

$$u_\alpha(\hat{k})k_\alpha = 0 \tag{7}$$

in place of (4) and

$$-i\omega u_\beta(\hat{k}) + ik_\mu\int u_\beta(\hat{q})u_\mu(\hat{k}-\hat{q})\frac{d\hat{q}}{(2\pi)^4} - \alpha g T(\hat{k})\delta_{\beta 3} = -ik_\beta\frac{P(\hat{k})}{\rho} - \nu_0 k^2 u_\beta(\hat{k}) + f^0_\beta(\hat{k}) \tag{8}$$

in place of (2), where $\hat{k}=(\omega,\mathbf{k})$, $\hat{q}=(\Omega,\mathbf{q})$, and $f^0_\beta(\hat{k})$ is the Fourier transform of the external forcing. One of the advantages of spectral representation of the equations of motion is its ability to eliminate the pressure term from the equations. Evaluate the pressure term by taking the divergence of (8) using the continuity equation (7),

$$-\frac{k_\mu k_\nu}{k^2}\int u_\mu(\hat{q})u_\nu(\hat{k}-\hat{q})\frac{d\hat{q}}{(2\pi)^4}-\frac{ik_3}{k^2}\alpha g T(\hat{k})=\frac{P(\hat{k})}{\rho}, \quad (9)$$

where the standard nonlinear term on the left side of (9) is now complemented by a new term that reflects the contribution of density stratification. Substituting Eq. (9) in (8) obtain

$$G_0^{-1}(\omega,\mathbf{k})u_\beta(\hat{k})=f_\beta^0(\hat{k})+\alpha g T(\hat{k})P_{3\beta}(\mathbf{k})-\frac{i}{2}P_{\beta\mu\nu}(\mathbf{k})\int u_\mu(\hat{q})u_\nu(\hat{k}-\hat{q})\frac{d\hat{q}}{(2\pi)^4}, \quad (10)$$

where

$$P_{ij}(\mathbf{k})=\delta_{ij}-k_ik_j/k^2, \quad (11)$$

$$P_{lmn}(\mathbf{k})=k_mP_{ln}(\mathbf{k})+k_nP_{lm}(\mathbf{k}), \quad (12)$$

$$G_0^{-1}(\omega,\mathbf{k})=-i\omega+\nu_0k^2, \quad (13)$$

$G_0(\omega,\mathbf{k})$ is the "bare" Green function, and δ_{ij} is the Kronecker δ symbol.

In the case of neutral stratification, Eq. (10) takes the canonical form

$$u_\beta(\hat{k})=G_0(\omega,\mathbf{k})f_\beta^0(\hat{k})-\frac{i}{2}G_0(\omega,\mathbf{k})P_{\beta\mu\nu}(\mathbf{k})\times\int u_\mu(\hat{q})u_\nu(\hat{k}-\hat{q})\frac{d\hat{q}}{(2\pi)^4}. \quad (14)$$

When stratification is present, Eq. (10) can be still reduced to the canonical form (14) by eliminating the temperature term using Fourier-transformed Eq. (3),

$$T(\hat{k})=G_{T0}(\hat{k})f_T(\hat{k})-iG_{T0}(\hat{k})k_\alpha\int u_\alpha(\hat{q})T(\hat{k}-\hat{q})\frac{d\hat{q}}{(2\pi)^4}, \quad (15)$$

where

$$f_T(\hat{k})=-\frac{d\Theta}{dz}u_3(\hat{k}) \quad (16)$$

assumes the role of the stochastic forcing and $G_{T0}(\hat{k})$ is the bare temperature Green function given by

$$G_{T0}(\omega,\mathbf{k})=(-i\omega+\kappa_0k^2)^{-1}. \quad (17)$$

Now, introduce a formal solution to Eq. (15) as a temperature Langevin equation,

$$T(\hat{k})=G_T(\hat{k})f_T(\hat{k}), \quad (18)$$

where $G_T(\hat{k})$ involves an effective diffusivity. Substituting Eq. (18) in (10), derive the canonical form of the velocity equation,

$$u_\beta(\hat{k})=G_{\alpha\beta}^0(\hat{k})f_\alpha^0(\hat{k})-\frac{i}{2}G_{\alpha\beta}^0(\hat{k})P_{\alpha\mu\nu}(\mathbf{k})\times\int u_\mu(\hat{q})u_\nu(\hat{k}-\hat{q})\frac{d\hat{q}}{(2\pi)^4}, \quad (19)$$

where the bare velocity Green function, $G_{\alpha\beta}^0(\hat{k})$, possesses a nondiagonal tensorial structure,

$$G_{\alpha\beta}^0(\omega,\mathbf{k})=G_0(\omega,\mathbf{k})[\delta_{\alpha\beta}+N^2G_T(\omega,\mathbf{k})\times G_0(\omega,\mathbf{k})P_{\alpha3}(\mathbf{k})\delta_{\beta3}]^{-1}. \quad (20)$$

Here, $N\equiv[\alpha g(d\Theta/dz)]^{1/2}$ is the buoyancy or Brunt-Väisälä frequency. The matrix on the right side of (20) can be inverted analytically for an arbitrary N yielding

$$G_{\alpha\beta}^0(\omega,\mathbf{k})=G_0(\omega,\mathbf{k})[\delta_{\alpha\beta}+A(\omega,\mathbf{k})P_{\alpha3}(\mathbf{k})\delta_{\beta3}], \quad (21)$$

where

$$A(\omega,\mathbf{k})=-\frac{N^2}{G_0^{-1}(\omega,\mathbf{k})G_T^{-1}(\omega,\mathbf{k})+N^2P_{33}(\mathbf{k})}. \quad (22)$$

The difference between Eqs. (14) and (19) is in the tensorial nature of the velocity Green function brought about by the effect of stable stratification. Accordingly, the Langevin equation (1) also acquires tensorial structure. Let us emphasize that the formal solution (18) made it possible to reduce Eq. (10) to the canonical form (19) which is self-contained for the velocity. The effective diffusivities in $G_T(\hat{k})$ will be found simultaneously with effective viscosities in the process of coarse graining. Since, as evident from Eq. (20), $G_{\alpha\beta}^0(\omega,\mathbf{k})$ involves $G_T(\hat{k})$, it is anticipated that equations for the effective viscosities and diffusivities form a coupled system. Sections II A–II D will describe a series of steps for solving that coupled system and calculating effective viscosities and diffusivities in the framework of the QNSE model.

A. Dynamic dissipation cutoff wave number

One of the key parameters here will be the dynamic dissipation cutoff Λ. This parameter is utilized in the scale elimination procedure aimed at accomplishing ensemble averaging of a small $\Delta\Lambda$ shell of modes in the vicinity of Λ and purge them from Eqs. (15) and (19). As a result, the effective dissipation wave number moves from Λ to its new value, $\Lambda-\Delta\Lambda$, while the viscosity and diffusivity gain $O(\Delta\Lambda)$ corrections $\Delta\nu$ and $\Delta\kappa$, respectively. The effective Re based upon the parameters in the vicinity of $\Lambda-\Delta\Lambda$ is, again, $O(1)$, such that a new $\Delta\Lambda$ shell of modes can be ensemble averaged and purged at the next iteration, and so on. The process of successive scale elimination starts at $\Lambda=k_d$ and can be continued until any predetermined wave number k_c is attained. When k_c is related to the numerical grid resolution in LES, $\nu(k_c)$ is the corresponding SGS viscosity. For convenience, all equations from now on will be understood as formulated in terms of Λ rather than k_d and accordingly, the subscript and superscript "0" will be omitted from all the Green functions implying the use of the effective viscosity and diffusivity, $\nu(\Lambda)$ and $\kappa(\Lambda)$, respectively.

B. "Slow" and "fast" modes

Development of a systematic procedure of successive small-scale elimination requires differentiation between the modes designated for purging and the rest of the modes. As elaborated earlier, Λ is the dynamic dissipation cutoff and $\Delta\Lambda$ is a thin shell, $\Delta\Lambda/\Lambda \ll 1$. Define the following domains: $D^<=(0,\Lambda-\Delta\Lambda]$, $D^>=(\Lambda-\Delta\Lambda,\Lambda]$, and $D=(0,\Lambda]=D^<\cup D^>$. Finally, the "slow" $(\mathbf{u}^<,T^<)$ and "fast" $(\mathbf{u}^>,T^>)$ velocity and temperature modes can be defined in such a way that $k\in D^<$ for $\mathbf{u}^<$ and $k\in D^>$ for $\mathbf{u}^>$. The subdivision of modes into slow and fast is equivalent to employing a sharp cutoff filter about $\Lambda-\Delta\Lambda$ which can be defined in terms of the Heaviside step-function θ,[25]

$$\theta^<(k)=\begin{cases}1 & \text{if } k\in D^<,\\ 0 & \text{if } k\in D^>,\end{cases} \tag{23}$$

and

$$\theta^>(k)=\begin{cases}0 & \text{if } k\in D^<,\\ 1 & \text{if } k\in D^>.\end{cases} \tag{24}$$

Then, the slow and fast velocity modes can be represented as

$$u_\alpha^<(\omega,\mathbf{k})=\theta^<(k)u_\alpha(\omega,\mathbf{k}), \tag{25}$$

$$u_\alpha^>(\omega,\mathbf{k})=\theta^>(k)u_\alpha(\omega,\mathbf{k}), \tag{26}$$

and a vector u_α can be decomposed into a sum, $u_\alpha=u_\alpha^<+u_\alpha^>$.

Similarly, the slow and fast temperature modes admit the following representation:

$$T^<(\omega,\mathbf{k})=\theta^<(k)T(\omega,\mathbf{k}), \tag{27}$$

$$T^>(\omega,\mathbf{k})=\theta^>(k)T(\omega,\mathbf{k}), \tag{28}$$

and $T=T^<+T^>$.

The nonlinearities in Eqs. (19) and (15) couple the fast and slow modes. Using Eq. (19), write down expressions for either $u_\alpha^<(\omega,\mathbf{k})$ or $u_\alpha^>(\omega,\mathbf{k})$,

$$u_\beta(\hat{k})=G_{\alpha\beta}(\hat{k})f_\alpha^0-\frac{i}{2}G_{\alpha\beta}(\hat{k})P_{\alpha\mu\nu}(\mathbf{k})\int[u_\mu^<(\hat{q})u_\nu^<(\hat{k}-\hat{q})+2u_\mu^>(\hat{q})u_\nu^<(\hat{k}-\hat{q})+u_\mu^>(\hat{q})u_\nu^>(\hat{k}-\hat{q})]\frac{d\hat{q}}{(2\pi)^4}. \tag{29}$$

Similarly, using Eq. (15), one can write down expressions for either $T^<(\omega,\mathbf{k})$ or $T^>(\omega,\mathbf{k})$,

$$T(\hat{k})=G_T(\hat{k})f_T(\hat{k})-iG_T(\hat{k})k_\alpha\int[u_\alpha^<(\hat{q})T^<(\hat{k}-\hat{q})+u_\alpha^<(\hat{q})T^>(\hat{k}-\hat{q})+u_\alpha^>(\hat{q})T^<(\hat{k}-\hat{q})+u_\alpha^>(\hat{q})T^>(\hat{k}-\hat{q})]\frac{d\hat{q}}{(2\pi)^4}. \tag{30}$$

For $k\in D^<$ and $k\in D^>$, Eqs. (29) and (30) describe $u_\beta^<,T^<$ and $u_\beta^>,T^>$, respectively. Equation for $u^<$ contains $u^>$ terms in the second (referred to as a cross term) and third terms of the integrand. Similarly, the equation for $T^<$ contains $T^>$ and/or $u^>$ terms in the second, third, and fourth terms of the integrand. The fast modes are eliminated from the equations for $u^<$ and $T^<$ by ensemble averaging with simultaneous adjustment of the effective viscosity and diffusivity and shrinking the spectral domain from D to $D^<$.

C. "Bare" versus "dressed" forces

Recall that the Langevin equations for the velocity,

$$u_\beta(\hat{k})=G_{\alpha\beta}(\hat{k})f_\alpha(\hat{k}), \tag{31}$$

involve the "dressed," or effective, force $f_\alpha(\hat{k})$ that accounts for the excitation of a single mode k by all other modes due to nonlinear interactions[15,16,19,26] and is quite different from the "bare" force $f_\alpha^0(\hat{k})$ that mimics the effect of large-scale instabilities and provides forcing that maintains turbulence. Numerous attempts to derive the dressed force from the first principles have failed so far[15,27] such that it has to be postulated. Let us now highlight the subtle connections between the bare and the postulated dressed forces.

In the spirit of the Kolmogorov theory of turbulence, it is usually assumed that the details of the bare force are not overly important as long as the force is solenoidal and concentrated on the large scales. Such force generates direct energy cascade that is characterized by the Kolmogorov spectrum. In the present model, $f_\alpha^0(\hat{k})$ in (19) is solenoidal and homogeneous in space and time such that its correlation function can be written as

$$\langle f_\alpha^0(\omega,\mathbf{k})f_\beta^0(\omega',\mathbf{k}')\rangle=D_0(\mathbf{k})\delta(\omega+\omega')\delta(\mathbf{k}+\mathbf{k}')P_{\alpha\beta}(\mathbf{k}). \tag{32}$$

Peaking at the largest scales of the flow, $f_\alpha^0(\omega,\mathbf{k})$ resembles the δ function, $D_0(\mathbf{k})\propto\delta(\mathbf{k})$. Utilizing the fact that the integral of (32) over all $\mathbf{k}$ determines the rate of the large-scale energy injection into the system, find $D_0(\mathbf{k})\propto\epsilon$. Invoking the power-law representation of the δ function in a three-dimensional space,[28] $\delta(\mathbf{k})=(1/4\pi)\lim_{\tau\to 0}\tau k^{-3+\tau}$, observe that the bare force correlator (32) has an infinitesimal amplitude for $k>0$,[29]

$$\langle f_\alpha^0(\omega,\mathbf{k})f_\beta^0(\omega',\mathbf{k}')\rangle\propto\tau k^{-3+\tau}\epsilon\delta(\omega+\omega')\times\delta(\mathbf{k}+\mathbf{k}')P_{\alpha\beta}(\mathbf{k}),\quad \tau\to 0. \tag{33}$$

Similar to the bare force, the dressed force is also solenoidal, zero mean, white noise in time, isotropic, and homogeneous in time and space, and its correlation function is given by

$$\langle f_\alpha(\omega,\mathbf{k})f_\beta(\omega',\mathbf{k}')\rangle=2D(2\pi)^4k^{-3}P_{\alpha\beta}(\mathbf{k})\delta(\omega+\omega')\times\delta(\mathbf{k}+\mathbf{k}'). \tag{34}$$

The dressed force is postulated to be Gaussian; its correlator (34) accounts for the statistically mean rate of energy input to a given mode k via its interaction with other modes. Thus, its amplitude D should be proportional to the mean rate of energy transfer through the mode k. Indeed, a relationship $D\simeq 15.7\epsilon$ has been derived for neutrally stratified flows.[18] A multiplicative factor k^{-3} in (34) ensures correct dimensionality. Several numerical coefficients are introduced for conve-

nience. Comparing (33) and (34), find that although both bare and dressed correlators scale with k^{-3}, their amplitudes are strikingly different being infinitesimal for the bare forcing and finite for the dressed forcing. Note also an important difference in the energetics of the bare and dressed forces. The former pertains to the global energy balance while the latter describes the forcing of a given mode only. Note that while the assumption of isotropy for the dressed force was well justified in neutral flows,[20] it may break down in flows with stratification. The anisotropization of the dressed force will be further discussed in Sec. VII.

D. The Feynman diagram method

To develop an algorithm of small-scale mode elimination it is convenient to use the Feynman diagram technique. To simplify the notations, the diagrams will be used in a loose sense suppressing tensorial indices. However, in the actual calculations, the tensorial nature of the diagrams is restored in order to obtain correct tensorial equations. Let us introduce the following diagrammatic notations for the canonical velocity equation (29):

$u_\beta(\hat{k})$ =

$G_{\alpha\beta}(\hat{k})$ =

$f^0_\alpha(\hat{k})$ = ×

$-\frac{i}{2}P_{\alpha\mu\theta}(\mathbf{k})\int\frac{d\hat{q}}{(2\pi)^4}$ = •

Equation (29) can be represented by the following diagram:

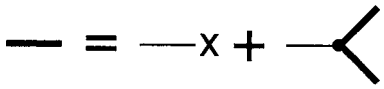

Analogous notations can be introduced for the temperature equation (30):

$T(\hat{k})$ =

$G_T(\hat{k})$ =

$f_T(\hat{k})$ = ⊗

$-ik_\alpha\int\frac{d\hat{q}}{(2\pi)^4}$ = ○

such that (30) can be represented by the diagram

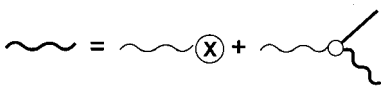

From now on, as a general rule, all lines denoting the fast range variables will be crossed by a short line. For instance, the slow and fast velocity modes are denoted as

$u^<_\alpha(\hat{k})$ =

$u^>_\alpha(\hat{k})$ =

Using Eq. (29), represent the equations for slow and fast velocity modes by the following diagrams:

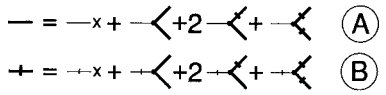

Diagram A contains fast modes in the third (cross term) and fourth terms on its right side. Iterate these terms one time by substituting diagram A in the cross term and diagram B in the fourth term,

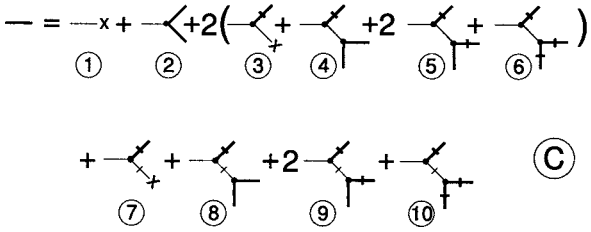

Diagram C is exact. Its various terms can be evaluated by applying the quasi-Gaussian approximation for the fast terms, i.e., by replacing all the fast velocity modes, represented by the thick crossed lines, by their respective Langevin equation (31) and performing averaging over the fast modes of the dressed force $\mathbf{f}^>$.[20] All diagrams containing odd moments of $\mathbf{f}^>$, i.e., 4, 6, 8, and 10, average out to zero. Diagram 3 represents a convolution of the kind $\int u^>(\hat{k}-\hat{q})\times G(\hat{q})f^0(\hat{q})d\mathbf{q}\propto u^>(\hat{k})$ by the δ-function nature of the bare force. But, since $k\in D^<$, $u^>(\hat{k})=0$ by definition of $u^>$, (26). Diagram 7 is also zero because it involves the bare force whose argument belongs in $D^>$. Thus, upon ensemble averaging over the fast modes, only diagrams 5 and 9 yield nontrivial contributions

(the cross-term contribution[20]) and

respectively. The sum of these diagrams gives correction to the inverse Green function that in turn provides corrections to effective viscosities due to coarse graining. Here, the thick half circle denotes the spectrum tensor $U_{\mu\sigma}(\Omega,\mathbf{q})$, $q\in D^>$, defined via the two-point, two-time velocity correlation function,

$$\langle u_\mu(\Omega,\mathbf{q})u_\sigma(\Omega',\mathbf{q}')\rangle=(2\pi)^4\delta(\mathbf{q}+\mathbf{q}')\times\delta(\Omega+\Omega')U_{\mu\sigma}(\Omega,\mathbf{q}). \tag{35}$$

Using Eqs. (31), (34), and (35), evaluate the spectrum tensor,

$$U_{\mu\sigma}(\hat{q})=2Dq^{-3}G_{\alpha\mu}(\hat{q})G^*_{\beta\sigma}(\hat{q})P_{\alpha\beta}(\mathbf{q}). \tag{36}$$

Usually, to derive diagram E, both crossed lines in the last term on the right side of A are iterated using B and only the lowest-order terms (i.e., diagrams with two vertices) are retained. This procedure would have yielded a coefficient 4 in E making it convenient to evaluate the sum of diagrams D and E. Here, an alternative procedure is adopted that does not rely on the expansion in powers of the nonlinear coupling. Represent the sum as

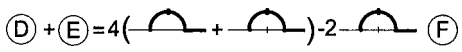

and take a note that the analytical expressions for both diagrams in the brackets are identical,

$$-\frac{1}{4}G_{\alpha\beta}(\hat{k})P_{\alpha\mu\theta}(\mathbf{k})u_{\beta}^{<}(\hat{k})\int P_{\nu\sigma\beta}(\mathbf{k}-\mathbf{q})U_{\mu\sigma}(\Omega,\mathbf{q}) \times G_{\theta\nu}(\omega-\Omega,\mathbf{k}-\mathbf{q})\frac{d\mathbf{q}d\Omega}{(2\pi)^4}, \tag{37}$$

albeit their integration domains are different. The first integral is computed over the intersection of $q\in D^{>}$ and $|\mathbf{k}-\mathbf{q}|\in D^{<}$ while the second integral is computed over the intersection of $q\in D^{>}$ and $|\mathbf{k}-\mathbf{q}|\in D^{>}$. These domains do not intersect so that the sum of the two integrals can be represented by a single integral over the union of their domains. This union is the intersection of $q\in D^{>}$ and $|\mathbf{k}-\mathbf{q}|\in D^{<}\cup D^{>}$ equal to the intersection $D^{>}\cap D$ or, simply, the shell $q\in D^{>}$ itself.

In the remaining integral in F the integration domain is the intersection of two spherical shells $D^{>}$ shifted by k relative to each other. This domain is $O[(\Delta\Lambda)^2]$ as the intersection of two $O(\Delta\Lambda)$ shells. Eventually, a limit $\Delta\Lambda\to 0$ will be taken such that the $O[(\Delta\Lambda)^2]$ terms should be neglected. This integral is not small only when $k<\Delta\Lambda$. However, this requirement is not fulfilled in general. While $\Delta\Lambda$ is, indeed, small, k does not need to be infinitesimal. In fact, the entire diagram E could be neglected as being $O[(\Delta\Lambda)^2]$ small. In other words, the main contribution to the ensemble-averaged Eq. (19) for the slow modes comes from the cross term. The contribution from diagram E has been retained only for the purpose of complementing the integration domain in (37) to the spherical shell $q\in D^{>}$ in order to simplify the integration.

The equation for the slow modes takes the form of the canonical equation (19) in which the inverse Green function, $G_{\alpha\beta}^{-1}(\omega,\mathbf{k})$, is modified as a result of the elimination of the shell $D^{>}$,

$$[G_{\alpha\beta}^{-1}(\hat{k})+\Delta G_{\alpha\beta}^{-1}(\hat{k})]u_{\beta}^{<}(\hat{k}) = f_{\alpha}^{0}(\hat{k})-\frac{i}{2}P_{\alpha\mu\theta}(\mathbf{k})\int u_{\mu}^{<}(\hat{q})u_{\theta}^{<}(\hat{k}-\hat{q})\frac{d\hat{q}}{(2\pi)^4}, \tag{38}$$

where

$$\Delta G_{\alpha\beta}^{-1}(\omega,\mathbf{k}) = P_{\alpha\mu\theta}(\mathbf{k})\int^{>} P_{\nu\sigma\beta}(\mathbf{k}-\mathbf{q}) \times U_{\mu\sigma}(\Omega,\mathbf{q})G_{\theta\nu}(\omega-\Omega,\mathbf{k}-\mathbf{q})\frac{d\mathbf{q}d\Omega}{(2\pi)^4} \tag{39}$$

and

$$\int^{>} d\hat{q} = \int_{D^{>}} d\mathbf{q}\int_{-\infty}^{\infty} d\Omega. \tag{40}$$

For transparency, it would be beneficial to explicitly account for the parametric dependence of $\Delta G_{\alpha\beta}^{-1}$ on the dynamic dissipation cutoff Λ and write $\Delta G_{\alpha\beta}^{-1}(\omega,\mathbf{k};\Lambda)$. The integral in (39) is calculated in the limits $\omega\to 0$ (only the long-time behavior is considered) and $k/\Lambda\to 0$ in which only the terms up to $O(k^2)$ are retained (the distant interaction approximation[18,19]). Although the validity of the distant interaction approximation cannot be proven rigorously at the present time, it can be justified using heuristic arguments.[19] Its utility is underscored by the fact that it provides an accurate description of the effective viscosity.[19] The distant interaction approximation will be adopted throughout this study. The parameter Λ will be omitted from the argument of $\Delta G_{\alpha\beta}^{-1}$ for brevity.

Applying the Feynman diagram method to the temperature equation (30), obtain diagrammatic equations for the slow and fast temperature modes, $T^{<}$ and $T^{>}$,

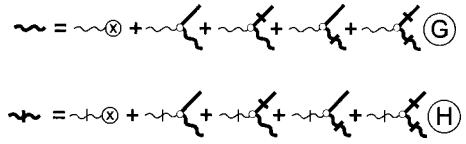

The right side of the diagram for $T^{<}$ contains five terms; those are the forcing $G_T f_T$, the conventional nonlinear term $u^{<}T^{<}$, the two cross terms $u^{>}T^{<}$ and $u^{<}T^{>}$, and the term $u^{>}T^{>}$. Similar to the case of velocity equation, the cross terms are iterated by substituting the slow mode diagrams, G and A, for $T^{<}$ and $u^{<}$, respectively, while the term $u^{>}T^{>}$ is iterated by substituting diagram H for $T^{>}$. As a result, the following diagram emerges:

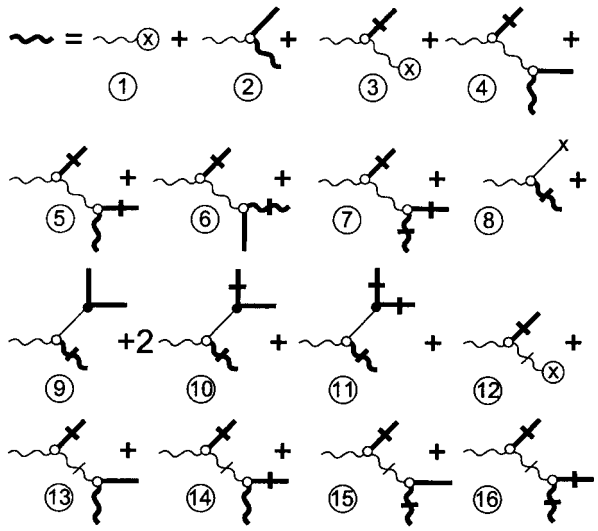

Similar to diagram C, this diagram is exact. Its ensemble average can be evaluated by replacing all the fast velocity and temperature modes, represented by the thick straight and wavy crossed lines, by their respective Langevin equations, (31) and (18), and performing averaging over the fast modes. All diagrams containing odd moments of $\mathbf{f}^{>}$, i.e., 4, 7, 9, 11, 13, and 16, average out of zero. Diagram 8 represents a convolution of the kind $\int T^{>}(\hat{k}-\hat{q})G(\hat{q})f^{0}(\hat{q})d\mathbf{q}\propto T^{>}(\hat{k})$ by the δ-function nature of the bare force. But, since $k\in D^{<}$, $T^{>}(\hat{k})=0$ by definition of $T^{>}$, Eq. (28). Diagrams 6, 10, and 15 are evaluated by substitution of Eqs. (16) and (18) that relate $u_3^{>}$ to $T^{>}$; they produce three types of diagrams,

These diagrams describe the thermodynamic corrections to the forcing term $G_T f_T$ which are $O(k^2)$ small. Diagrams 3 and 12 are evaluated by substituting Eq. (16) that relates f_T to $u_3(\hat{k})$ and then diagram A for $u_3^<$ in 3 and diagram B for $u_3^>$ in 12. The ensuing diagrams are of the second and third types as shown above and thus produce additional thermodynamic corrections to the forcing term $G_T f_T$ which are $O(k^2)$ small. At the final account, only two diagrams, 5 and 14, generate a nontrivial correction to the right side of diagram G after elimination of the fast shell $D^>$; this correction is given by the following diagrammatic sum:

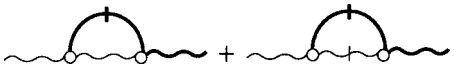

The analytical expression for this sum is

$$-G_T(\hat{k})k_\alpha k_\beta T^<(\hat{k})\int^> U_{\alpha\beta}(\Omega,\mathbf{q})G_T(\omega-\Omega,\mathbf{k}-\mathbf{q})\frac{d\mathbf{q}d\Omega}{(2\pi)^4}, \tag{41}$$

where the integration domain is a spherical shell $D^>$ defined in (40). Similar to the case of the coarse graining of the velocity diagram A, the second diagram complements the integration domain in (41) precisely to the spherical shell $D^>$.

Finally, these results can be recast in terms of the correction to the inverse temperature Green function G_T^{-1} in the coarse-grained Eq. (15) after one iteration,

$$[G_T^{-1}(\hat{k})+\Delta G_T^{-1}(\hat{k})]T^<(\hat{k}) = f_T(\hat{k}) - ik_\alpha\int u_\alpha^<(\hat{q}) \times T^<(\hat{k}-\hat{q})\frac{d\hat{q}}{(2\pi)^4}, \tag{42}$$

where

$$\Delta G_T^{-1}(\omega,\mathbf{k}) = k_\alpha k_\beta\int^> U_{\alpha\beta}(\Omega,\mathbf{q})G_T(\omega-\Omega,\mathbf{k}-\mathbf{q})\frac{d\mathbf{q}d\Omega}{(2\pi)^4}. \tag{43}$$

Similar to Eq. (39), the integral in (43) is calculated invoking the limit $\omega\to 0$ and the distant interaction approximation which give rise to corrections to the effective diffusivity due to the coarse graining.

E. Effective viscosity in case of neutral stratification

In the case of neutral stratification, the velocity Green function is essentially a scalar given by (13); the correction to the inverse Green function [i.e., Eq. (39)] simplifies to

$$\Delta G^{-1}(\hat{k})\delta_{\alpha\beta} = 2DG(\hat{k})P_{\alpha\mu\theta}(\mathbf{k})\int^> |G(\hat{q})|^2 G(\hat{k}-\hat{q}) \times P_{\theta\sigma\beta}(\mathbf{k}-\mathbf{q})P_{\sigma\mu}(\mathbf{q})q^{-3}\frac{d\hat{q}}{(2\pi)^4}. \tag{44}$$

The term $\Delta G^{-1}(\hat{k})$ is the direct result of elimination of the fast shell $D^>$ and, thus, reflects the impact of this shell upon the remaining slow modes. Taking the limit $\omega\to 0$ and invoking the distant interaction approximation, calculate correction to the effective viscosity resulting from the elimination of the shell $D^>$,

$$\Delta\nu_n = -A_d\frac{D}{\nu_n^2\Lambda^5}\Delta\Lambda, \tag{45}$$

where

$$A_d = \frac{\tilde{A}_d}{2\pi^2}, \quad \tilde{A}_d = \frac{d-1}{2(d+2)}, \tag{46}$$

and $d=3$ is the spatial dimension[20] (in the forthcoming derivations, the effective viscosity in the neutral case will carry the subscript n: ν_n). Equation (45) completes one iteration in the process of small-scale mode elimination.

In the limit $\Delta\Lambda\to 0$, one obtains a differential equation,

$$\frac{d\ln\nu_n}{d\ln\Lambda} = -\frac{A_d D}{\nu_n^3(\Lambda)\Lambda^4}, \tag{47}$$

which can be solved subject to the boundary condition $\nu_n(\Lambda_0)=\nu_0$, $\Lambda_0=k_d$. For $\Lambda\ll k_d$, the asymptotic value of $\nu_n(\Lambda)$ is

$$\nu_n(\Lambda) \simeq \left(\frac{3A_d D}{4}\right)^{1/3}\Lambda^{-4/3} \simeq (0.0076D)^{1/3}\Lambda^{-4/3}. \tag{48}$$

These and other results (the derivation of the Kolmogorov spectrum, the calculation of the Kolmogorov and Batchelor constants, etc.) as well as the technique of the small-scale mode elimination are basically the same as in the RG theory of turbulence.[17–19] However, in the QNSE model these results are obtained via quasi-Gaussian mapping of the velocity field using the Langevin equation (31) with the postulated dressed force $f_\alpha(\hat{k})$ and without explicit resorting to the ϵ expansion and fixed-point arguments that are central to the RG theory. In addition, retaining the cross term in the equation for $\mathbf{u}^<$ and evaluating the integral in (39) over the shell $D^>$ have resulted in the disappearance of the parameter $\epsilon=4$ of the ϵ expansion from the amplitude of the effective viscosity, $\tilde{A}_d$ in (46).[20]

When stable stratification is present, the computation of the integrals in (39) and (43) is hampered by anisotropy. This problem will be dealt with in Secs. III–V. The calculations have been assisted by the use of symbolic computer language MATHEMATICA™.

III. HORIZONTAL AND VERTICAL EFFECTIVE VISCOSITIES AND DIFFUSIVITIES

The calculation of the integrals in (39) and (43) detailed in Secs. IV and V will yield corrections to the inverse velocity and temperature Green functions. Due to the anisotropy introduced by stable stratification, the effective viscosities and diffusivities will be shown to transform differently in the directions parallel and orthogonal to the direction of stratification. Stable stratification breaks the isotropy of the flow in the vertical but leaves it intact in the horizontal direction. To

take advantage of this in the calculations, we will distinguish between the horizontal (k_h) and vertical ($k_z \equiv k_3$) wave numbers,

$$k^2 = k_1^2 + k_2^2 + k_3^2 = k_h^2 + k_3^2, \tag{49}$$

and between the horizontal (ν_h, κ_h) and vertical (ν_z, κ_z) effective viscosities and diffusivities, which, for the future convenience, can be written as

$$\nu_h \equiv \nu, \quad \nu_z = \nu + \delta\nu_z, \tag{50}$$

$$\kappa_h \equiv \kappa, \quad \kappa_z = \kappa + \delta\kappa_z. \tag{51}$$

Then, the spectral viscosity and diffusivity operators become

$$\nu_h k_h^2 + \nu_z k_z^2 = \nu k^2 + \delta\nu_z k_3^2, \tag{52}$$

$$\kappa_h k_h^2 + \kappa_z k_z^2 = \kappa k^2 + \delta\kappa_z k_3^2, \tag{53}$$

and the scalar Green functions can be defined as

$$G(\omega,k,k_3) = (-i\omega + \nu k^2 + \delta\nu_z k_3^2)^{-1}, \tag{54}$$

$$G_T(\omega,k,k_3) = (-i\omega + \kappa k^2 + \delta\kappa_z k_3^2)^{-1}. \tag{55}$$

Prior to the initiation of the scale elimination process, the values on the right side of these equations are $\nu=\nu_0$, $\kappa=\kappa_0$, $\delta\nu_z=0$, and $\delta\kappa_z=0$.

In Secs. IV and V, it will be shown that the corrections to the inverse velocity and temperature Green functions due to elimination of the fast shell $D^>$ have the following form:

$$\Delta G_{\alpha\beta}^{-1}(0,\mathbf{k}) = \delta_{\alpha\beta}(k^2\Delta\nu + k_3^2\Delta\delta\nu_z) + \delta_{\beta 3}\Delta V_{\alpha 3}, \tag{56}$$

$$\Delta G_T^{-1}(0,\mathbf{k}) = k^2\Delta\kappa + k_3^2\Delta\delta\kappa_z, \tag{57}$$

where $\Delta\nu$, $\Delta\delta\nu_z$, $\Delta\kappa$, $\Delta\delta\kappa_z$, and $\Delta V_{\alpha 3}$ are all $O(\Delta\Lambda)$. Note that the correction to the inverse Green function, $\Delta G_{\alpha\beta}^{-1}$, preserves the tensorial structure of $G_{\alpha\beta}^{-1}$, and the corrections to the effective viscosities and diffusivities preserve the form of the respective inverse Green functions (54) and (55). The off-diagonal term $\Delta V_{\alpha 3}$ in (56) is comprised of the terms proportional to k^2 and k_3^2 which are structurally similar to the horizontal and vertical viscosities. On the other hand, the off-diagonal term is proportional to $k^2 N$ which can be interpreted as a small correction to the Brunt-Väisälä frequency N. Hence, this term does not affect the calculation of the diagonal terms. Although these off-diagonal terms may be important in some situations,[30] their consideration is beyond the scope of the present study.

The tensorial velocity Green function, Eq. (21), can be written in the new notations as

$$G_{\alpha\beta}(\omega,k,k_3) = G(\omega,k,k_3)[\delta_{\alpha\beta} + A(\omega,k,k_3)P_{\alpha 3}(\mathbf{k})\delta_{\beta 3}], \tag{58}$$

where

$$A(\omega,k,k_3) = -N^2[(-i\omega + \nu k^2 + \delta\nu_z k_3^2) \times (-i\omega + \kappa k^2 + \delta\kappa_z k_3^2) + N^2 P_{33}(\mathbf{k})]^{-1}. \tag{59}$$

Evaluate the energy spectrum tensor (36) using (58) and (59),

$$U_{\alpha\beta}(\omega,k,k_3) = 2Dk^{-3}|G(\omega,k,k_3)|^2 \times [P_{\alpha\beta}(\mathbf{k}) + B(\omega,k,k_3)P_{\alpha 3}(\mathbf{k})P_{\beta 3}(\mathbf{k})], \tag{60}$$

where

$$B(\omega,k,k_3) = A(\omega,k,k_3) + A^*(\omega,k,k_3) + |A(\omega,k,k_3)|^2 P_{33}(\mathbf{k}). \tag{61}$$

The explicitly anisotropic variables introduced in this section significantly simplify the calculation of the effective transport coefficients in stably stratified flows detailed in Secs. IV and V.

IV. COMPUTATION OF THE EFFECTIVE DIFFUSIVITIES

Evaluation of the integrals in Eqs. (39) and (43) includes the following steps:

(A) Contour integration over the frequency Ω;
(B) making use of the distant interaction approximation;
(C) integration over the spherical shell $D^>$ which combines multiplication by $\Delta\Lambda$ and the angular integration over the surface of the sphere with the radius Λ.

The inherent anisotropy due to stable stratification complicates this angular integration. However, utilizing isotropy of the integrand in the horizontal plane allows to carry out most of the calculations analytically.

In order to reduce the algebraic burden and make the computation procedure more transparent to the reader, the integral in (43) will be calculated first. Then, we will present a compressed calculation of the integral in (39) placing the lengthier algebraic expressions in Appendixes.

Another general remark needs to be made. In the forthcoming calculations, the continuity equation (7) will be routinely enforced, i.e., since the integral (39) is factored with $u_\beta(\hat{k})$, any term in the integral that is proportional to k_β will be set to zero automatically. Other simplifying relationships are related to the symmetry and solenoidality properties of the projection operator, $P_{\alpha\beta}(\mathbf{k}) = P_{\beta\alpha}(\mathbf{k})$ and $k_\alpha P_{\alpha\beta}(\mathbf{k}) = 0$. All the related simplifications will be implemented without specific mentioning.

Let us now turn to Eq. (43) where the integrand is

$$I_{\alpha\beta}^T = U_{\alpha\beta}(\Omega,q,q_3)G_T(\omega-\Omega,|\mathbf{k}-\mathbf{q}|,k_3-q_3). \tag{62}$$

According to the distant interaction approximation, the calculation of the expression in the right side of (43) needs to be carried out only up to the order of $O(k^2)$. Due to the presence of the product $k_\alpha k_\beta$ in front of the integral in (43), only the $O(1)$ terms should be retained in the integrand (62) such that one can set $k=0$ and $k_3=0$ in G_T yielding

$$I_{\alpha\beta}^T = U_{\alpha\beta}(\Omega,q,q_3)G_T(\omega-\Omega,q,q_3). \tag{63}$$

Using Eq. (60) one can represent $I_{\alpha\beta}^T$ as a product,

$$I_{\alpha\beta}^T = 2Dq^{-3}G_T(\omega-\Omega,q,q_3)G(\Omega,q,q_3)G(-\Omega,q,q_3) \times [P_{\alpha\beta}(\mathbf{q}) + B(\Omega,q,q_3)P_{3\alpha}(\mathbf{q})P_{3\beta}(\mathbf{q})]. \tag{64}$$

Recall that since only long-term flow properties are of inter-

est here, Eq. (64) is considered in the limit $\omega \to 0$.

Inspection of Eq. (64) reveals that it contains scalar factors that depend on Ω and tensorial factors that are independent of Ω. Therefore, the integrand $I^T_{\alpha\beta}$ can be represented as a factorized sum,

$$I^T_{\alpha\beta} = 2Dq^{-3}\sum_{i=1}^{2} T^i_{\alpha\beta}(\mathbf{q}) S^i(\Omega, q, q_3), \tag{65}$$

where

$$T^1_{\alpha\beta}(\mathbf{q}) = P_{\alpha\beta}(\mathbf{q}), \tag{66}$$

$$T^2_{\alpha\beta}(\mathbf{q}) = P_{3\alpha}(\mathbf{q}) P_{3\beta}(\mathbf{q}), \tag{67}$$

$$S^1(\Omega, q, q_3) = G_T(-\Omega, q, q_3) G(\Omega, q, q_3) G(-\Omega, q, q_3), \tag{68}$$

$$S^2(\Omega, q, q_3) = S^1(\Omega, q, q_3) B(\Omega, q, q_3). \tag{69}$$

The factorized representation (65) significantly simplifies the forthcoming calculations because the frequency integration involves only the scalar functions.

At this point, the preconditioning of the integrand is completed and the integral in (43) can be calculated following the steps A, B, and C outlined earlier.

A. Frequency integration

The Ω-integration of the scalar functions $S^1(\Omega, q, q_3)$ and $S^2(\Omega, q, q_3)$ in (65) will be performed next using the contour methods.

1. Contribution from $S^1(\Omega, q, q_3)$

This term produces three poles,

$$\Omega_1 = i\omega^T_q, \quad \Omega_{2,3} = \pm i\omega_q, \tag{70}$$

where

$$\omega^T_q \equiv \kappa q^2 + \delta\kappa_z q_3^2, \tag{71}$$

$$\omega_q \equiv \nu q^2 + \delta\nu_z q_3^2. \tag{72}$$

Two of these poles, Ω_1 and Ω_2, are located in the upper half plane while Ω_3 belongs in the lower half plane. The frequency integral R^1 is computed using the residue at the pole Ω_3 yielding

$$R^1(q, q_3) = \int S^1(\Omega, q, q_3) \frac{d\Omega}{2\pi} = \frac{1}{2\omega_q(\omega_q + \omega^T_q)}. \tag{73}$$

2. Contribution from $S^2(\Omega, q, q_3)$

This term produces seven poles, three of which are given by Eq. (70) and the rest, due to the factor $B(\Omega, q, q_3)$, are

$$\Omega_{4,5,6,7} = \pm \frac{i}{2}(\omega_q + \omega^T_q) \pm \frac{1}{2}\sqrt{4N^2 P_{33}(\mathbf{q}) - (\omega_q - \omega^T_q)^2}. \tag{74}$$

Four of these seven poles, Ω_1, Ω_2, Ω_4, and Ω_6, are located in the upper half plane while the remaining three belong in the lower half plane. The frequency integral R^2 is calculated using the residues at the latter poles yielding

$$R^2(q, q_3) = \int S^2(\Omega, q, q_3) \frac{d\Omega}{2\pi} = \frac{-N^2}{2\omega_q(\omega_q + \omega^T_q)[N^2 P_{33}(\mathbf{q}) + \omega_q \omega^T_q]}. \tag{75}$$

The frequency integration in (43) is now completed and the result is

$$\int I^T_{\alpha\beta} \frac{d\Omega}{2\pi} = 2Dq^{-3}\sum_{i=1}^{2} T^i_{\alpha\beta}(\mathbf{q}) R^i(q, q_3). \tag{76}$$

The angular integration is described next.

B. Distant interaction approximation

The distant interaction approximation makes it possible to isolate terms that generate effective viscosities and diffusivities and to simplify the angular integration. Recall that in this approximation, only the terms up to $O[(k/\Lambda)^2]$ are retained in ΔG_T^{-1}. In fact, this approximation has already been applied to Eq. (62) when k and k_3 were set to zero due to the presence of the factor $k_\alpha k_\beta$ in front of the integral in (43). It is useful to show here the expressions for the contraction of the factor $k_\alpha k_\beta$ with $T^1_{\alpha\beta}$ and $T^2_{\alpha\beta}$ although these products are already $O(k^2)$ and do not require any additional simplifications,

$$k_\alpha k_\beta T^1_{\alpha\beta}(\mathbf{q}) = k_\alpha k_\beta P_{\alpha\beta}(\mathbf{q}) = k^2 - \frac{k_\alpha k_\beta q_\alpha q_\beta}{q^2}, \tag{77}$$

$$k_\alpha k_\beta T^2_{\alpha\beta}(\mathbf{q}) = k_\alpha k_\beta P_{3\alpha}(\mathbf{q}) P_{3\beta}(\mathbf{q}) = k_3^2 - \frac{2k_3 q_3 k_\alpha q_\alpha}{q^2} + \frac{q_3^2 k_\alpha k_\beta q_\alpha q_\beta}{q^4}. \tag{78}$$

C. Integration over the spherical shell $D^>$

The integration of expression (76) over a spherical shell $D^>$ consists of the integration in the radial direction (which just means multiplication of the integrand by $-\Delta\Lambda$; the negative sign is due to compression of the domain when scales are eliminated) and subsequent integration over the surface of a d-dimensional sphere, Σ_d, with a radius Λ (it is convenient to perform some of the calculations in the d-dimensional space with the understanding that $d=3$). In the isotropic case, the angular integration would be straightforward yielding the sums of the products of the Kronecker δ symbols.[18,20] In flows with stable stratification, however, the integrand (76) is anisotropic and the procedure of angular integration needs further development. Inspecting this integrand with account of Eqs. (77) and (78), observe that it is comprised of the products of terms, some of which depend on q_3 only (these terms are due to the residues R^1 and R^2) while others, produced by the tensorial functions $T^1_{\alpha\beta}$ and $T^2_{\alpha\beta}$, involve a polynomial dependence on the scalar products of the type $k_\alpha q_\alpha$. The latter terms preserve the isotropy in the horizontal plane. Taking advantage of this observation, one

can perform the angular integration over the surface of a d-dimensional sphere Σ_d by, first, integrating over the surface of a $d-1$-dimensional sphere Σ_{d-1} (for $d-1=2$, such a sphere is a circle in the horizontal plane) and, second, integrating over the vertical semicircle:

$$\int_{D^>} d^d q = -\Delta\Lambda \int_{\Sigma_d} d^{d-1} q = -\Lambda\Delta\Lambda \int_0^\pi d\theta \int_{\Sigma_{d-1}} d^{d-2} q. \tag{79}$$

Note that in the integration over Σ_{d-1}, the horizontal radius q_h is a function of the vertical coordinate given by

$$q_h = q \sin\theta = \Lambda \sin\theta, \tag{80}$$

where θ is the angle between the vector $\mathbf{q}$ and the vertical axis; q is replaced by Λ reflecting the fact that $D^>$ is a spherical shell of the radius Λ. By definition of the projection operator (11), one finds

$$P_{33}(\mathbf{q}) = 1 - q_3^2/q^2 = \sin^2\theta. \tag{81}$$

Due to the horizontal isotropy of the integrand (76), the integration over Σ_{d-1} can be performed analytically after representing the vector $\mathbf{q}$ as a sum of its horizontal, $\mathbf{q}_h = (q_1, q_2, 0)$, and vertical, q_3, projections,

$$q_j = q_{hj} + q_3 \delta_{3j}. \tag{82}$$

The integration over a $d-1$-dimensional spherical surface of the radius Λ can be accomplished by utilizing the following auxiliary relationships valid for the horizontal components of the vector $\mathbf{q}$,

$$\int_{\Sigma_{d-1}} d^{d-2} q = S_{d-1} (\Lambda \sin\theta)^{d-2}, \tag{83}$$

$$\int_{\Sigma_{d-1}} q_{h_\alpha} q_{h_b} d^{d-2} q = S_{d-1} (\Lambda \sin\theta)^d \frac{\delta_{\alpha\beta}}{d-1}, \tag{84}$$

$$\int_{\Sigma_{d-1}} q_{h_\alpha} q_{h_\beta} q_{h_\gamma} q_{h_\delta} d^{d-2} q = S_{d-1} (\Lambda \sin\theta)^{d+2} \times \frac{\delta_{\alpha\beta}\delta_{\gamma\delta} + \delta_{\alpha\gamma}\delta_{\beta\delta} + \delta_{\alpha\delta}\delta_{\beta\gamma}}{(d-1)(d+1)}, \tag{85}$$

where $S_d = 2\pi^{d/2}/\Gamma(d/2)$ is the surface area of a d-dimensional unit sphere, and α through δ are indices in the horizontal plane.

Substituting (82) in (77) and (78) and expanding the products, obtain

$$k_\alpha k_\beta T^1_{\alpha\beta}(\mathbf{q}) = k^2 - \frac{k_3^2 q_3^2}{q^2} - \frac{2k_3 q_3 k_\alpha q_{h\alpha}}{q^2} - \frac{k_\alpha k_\beta q_{h\alpha} q_{h\beta}}{q^2}, \tag{86}$$

$$k_\alpha k_\beta T^2_{\alpha\beta}(\mathbf{q}) = k_3^2 - \frac{2k_3^2 q_3^2}{q^2} + \frac{k_3^2 q_3^4}{q^4} - \frac{2k_3 q_3 k_\alpha q_{h\alpha}}{q^2} + \frac{2k_3 q_3^3 k_\alpha q_{h\alpha}}{q^4} + \frac{q_3^2 k_\alpha k_\beta q_{h\alpha} q_{h\beta}}{q^4}. \tag{87}$$

Using (86) and (87) along with the auxiliary relationships for the integration in the horizontal plane, obtain

$$\int_{\Sigma_{d-1}} k_\alpha k_\beta T^1_{\alpha\beta}(\mathbf{q}) d^{d-2} q = S_{d-1} (\Lambda \sin\theta)^{d-2} \left\{ k^2 \left[1 + \frac{\sin^2\theta}{d-1} \right] + k_3^2 \left[\frac{d \sin^2\theta}{d-1} - 1 \right] \right\}, \tag{88}$$

$$\int_{\Sigma_{d-1}} k_\alpha k_\beta T^2_{\alpha\beta}(\mathbf{q}) d^{d-2} q = S_{d-1} (\Lambda \sin\theta)^{d-2} \left[k^2 \frac{\sin^2\theta \cos^2\theta}{d-1} + k_3^2 \sin^2\theta \frac{d \sin^2\theta - 1}{d-1} \right]. \tag{89}$$

Equations (88) and (89) confirm that the tensorial structure was not violated during this calculation so that ΔG_T^{-1} can be represented in the format (57),

$$\Delta G_T^{-1} = k^2 \Delta\kappa + k_3^2 \Delta\kappa_z.$$

Finally, collect all the factors, take the limit $\Delta\Lambda \to 0$, substitute $d=3$, and obtain differential equations for κ and κ_z,

$$\frac{d\kappa}{d\Lambda} = -\frac{D}{8\pi^2\Lambda} \int_0^\pi \frac{[N^2 \sin^2\theta + (2 - \sin^2\theta)\omega_\Lambda \omega_\Lambda^T] \sin\theta}{\omega_\Lambda (\omega_\Lambda + \omega_\Lambda^T)(N^2 \sin^2\theta + \omega_\Lambda \omega_\Lambda^T)} d\theta, \tag{90}$$

$$\frac{d\kappa_z}{d\Lambda} = -\frac{D}{4\pi^2\Lambda} \int_0^\pi \frac{\omega_\Lambda^T \sin^3\theta}{(\omega_\Lambda + \omega_\Lambda^T)(N^2 \sin^2\theta + \omega_\Lambda \omega_\Lambda^T)} d\theta, \tag{91}$$

where

$$\omega_\Lambda \equiv \Lambda^2 (\nu + \delta\nu_z \cos^2\theta), \tag{92}$$

$$\omega_\Lambda^T \equiv \Lambda^2 (\kappa + \delta\kappa_z \cos^2\theta). \tag{93}$$

Equations (90) and (91) are coupled; their right sides involve both effective diffusivities and viscosities. Two additional differential equations, for ν and ν_z, will be derived in Sec. V. Even though the integrals on the right sides of all four equations cannot be taken analytically, they can be computed numerically using the values of the effective viscosities and diffusivities accumulated at Λ.

V. COMPUTATION OF THE EFFECTIVE VISCOSITIES

Equations for ν and $\delta\nu_z$ will be derived in this section using exactly the same steps and algorithms as those used above to obtain the effective diffusivities.

A. Frequency integration

It is convenient to bring the factor $P_{\alpha\mu\theta}(\mathbf{k})$ inside the integral in (39) and represent the integrand as

$$I_{\alpha\beta} = P_{\alpha\mu\theta}(\mathbf{k})P_{\nu\sigma\beta}(\mathbf{k}-\mathbf{q}) \times G_{\theta\nu}(\omega-\Omega,|\mathbf{k}-\mathbf{q}|,k_3-q_3)U_{\mu\sigma}(\Omega,q,q_3). \quad (94)$$

Substitute Eq. (21) for the Green function and (60) for the velocity correlator in (94) and represent the integrand as a factorized sum,

$$I_{\alpha\beta} = 2Dq^{-3}P_{\alpha\mu\theta}(\mathbf{k})\sum_{i=1}^{4} T^i_{\mu\theta\beta}S^i, \quad (95)$$

where the tensorial terms are

$$T^1_{\mu\theta\beta} = P_{\mu\sigma}(\mathbf{q})[k_\sigma P_{\theta\beta}(\mathbf{k}-\mathbf{q}) - P_{\theta\sigma}(\mathbf{k}-\mathbf{q})q_\beta], \quad (96)$$

$$T^2_{\mu\theta\beta} = P_{\mu\sigma}(\mathbf{q})P_{3\theta}(\mathbf{k}-\mathbf{q})[k_\sigma P_{3\beta}(\mathbf{k}-\mathbf{q}) - P_{3\sigma}(\mathbf{k}-\mathbf{q})q_\beta], \quad (97)$$

$$T^3_{\mu\theta\beta} = P_{3\mu}(\mathbf{q})P_{3\sigma}(\mathbf{q})[k_\sigma P_{\theta\beta}(\mathbf{k}-\mathbf{q}) - P_{\theta\sigma}(\mathbf{k}-\mathbf{q})q_\beta - P_{\theta\beta}(\mathbf{k}-\mathbf{q})q_\sigma], \quad (98)$$

$$T^4_{\mu\theta\beta} = P_{3\mu}(\mathbf{q})P_{3\sigma}(\mathbf{q})P_{3\theta}(\mathbf{k}-\mathbf{q})[k_\sigma P_{3\beta}(\mathbf{k}-\mathbf{q}) - P_{3\sigma}(\mathbf{k}-\mathbf{q})q_\beta - P_{3\beta}(\mathbf{k}-\mathbf{q})q_\sigma], \quad (99)$$

and the scalar terms, in the limit $\omega\to 0$, are

$$S^1 = \tilde{G}, \quad (100)$$

$$S^2 = \tilde{G}A, \quad (101)$$

$$S^3 = \tilde{G}B, \quad (102)$$

$$S^4 = \tilde{G}AB, \quad (103)$$

where $\tilde{G}=G(-\Omega,q,q_3)G(\Omega,q,q_3)G(-\Omega,|\mathbf{k}-\mathbf{q}|,k_3-q_3)$, $A=A(-\Omega,|\mathbf{k}-\mathbf{q}|,k_3-q_3)$, and $B=B(\Omega,q,q_3)$.

Similar to the case of the temperature equation (65), only the scalar functions S^i are Ω dependent; they generate a set of poles in the frequency integration in (39) whose contribution can be calculated using standard contour methods. The tensorial terms, on the other hand, only affect the angular integration. The contour integration is performed next.

1. Contribution from S^1

This term produces three poles,

$$\Omega_{1,2} = \pm i\omega_q, \quad \Omega_3 = i\omega_{k-q}, \quad (104)$$

where ω_q is given by Eq. (72) and

$$\omega_{k-q} \equiv \nu|\mathbf{k}-\mathbf{q}|^2 + \delta\nu_z(k_3-q_3)^2. \quad (105)$$

Two of these poles, Ω_1 and Ω_3, are located in the upper half plane while Ω_2 belongs in the lower half plane. The frequency integral $R^1(k,k_3,q,q_3)$ (for brevity, the arguments of R^i will be suppressed thereon) is computed using the residue at pole Ω_2 yielding

$$R^1 = \int S^1(\Omega,k,k_3,q,q_3)\frac{d\Omega}{2\pi} = \frac{1}{2\omega_q(\omega_{k-q}+\omega_q)}. \quad (106)$$

2. Contribution from S^2

The product of $\tilde{G}$ and the factor A, Eq. (22), produces, in addition to the three poles of S^1, two more complex poles in the upper half plane,

$$\Omega_{4,5} = \frac{i}{2}(\omega_{k-q}+\omega^T_{k-q}) \pm \frac{1}{2}\sqrt{4N^2P_{33}(\mathbf{k}-\mathbf{q}) - (\omega_{k-q}-\omega^T_{k-q})^2}, \quad (107)$$

where

$$\omega^T_{k-q} \equiv \kappa|\mathbf{k}-\mathbf{q}|^2 + \delta\kappa_z(k_3-q_3)^2. \quad (108)$$

Thus, function S^2 has five poles given by (104) and (107); four of them are located in the upper and one in the lower half plane. The frequency integral R^2 is computed using the residue at pole Ω_2:

$$R^2 = \int S^2(\Omega,k,k_3,q,q_3)\frac{d\Omega}{2\pi} = -R^1\frac{N^2}{(\omega_{k-q}+\omega_q)(\omega_q+\omega^T_{k-q}) + N^2P_{33}(\mathbf{k}-\mathbf{q})}. \quad (109)$$

3. Contribution from S^3

The function B given by (61) has the same poles as A and its conjugate A^* except that now $\mathbf{k}=0$ in the argument of A,

$$\Omega_{6,7,8,9} = \pm\frac{i}{2}(\omega_q+\omega^T_q) \pm \frac{1}{2}\sqrt{4N^2P_{33}(\mathbf{q}) - (\omega_q-\omega^T_q)^2}, \quad (110)$$

where ω^T_q is given by Eq. (71). Thus, S^3 has seven poles as given by Eqs. (104) and (110); four of these poles are located in the upper and three in the lower half plane. The frequency integral is computed using the residues at the lower half-plane poles and the result is

$$R^3 = \int S^3(\Omega,k,k_3,q,q_3)\frac{d\Omega}{2\pi} = -N^2R^1\frac{N^2P_{33}(\mathbf{q})(\omega_q+\omega_q^T)+\omega_q^T[\omega_{k-q}{}^2+2\omega_q(\omega_q+\omega_q^T)+\omega_{k-q}(2\omega_q+\omega_q^T)]}{(\omega_q+\omega_q^T)[N^2P_{33}(\mathbf{q})+\omega_q\omega_q^T][N^2P_{33}(\mathbf{q})+(\omega_{k-q}+\omega_q)(\omega_{k-q}+\omega_q^T)]}. \quad (111)$$

4. Contribution from S^4

The poles of the product $\tilde{G}AB$ are the union of all the poles given by (104), (107), and (110); thus, the function S^4 has nine poles, six of them located in the upper and three in the lower half plane. As in all other cases, the frequency integral is computed using the residues at the lower half-plane poles, yielding a full expression for

$$R^4 = \int S^4(\Omega,k,k_3,q,q_3)\frac{d\Omega}{2\pi} \quad (112)$$

that is given in Appendix A.

Upon completing the frequency integration, the integrand in the remaining integral over the spherical shell $D^>$ takes the form

$$I_{\alpha\beta} = 2Dq^{-3}P_{\alpha\mu\theta}(\mathbf{k})\sum_{i=1}^{4} T^i_{\mu\theta\beta}R^i. \quad (113)$$

B. Distant interaction approximation

Let us simplify the integrand (113) by retaining only the terms up to $O[(k/\Lambda)^2]$. Unlike the case of temperature equation, where the integral in (43) was factored with an $O(k^2)$ term and the integrand required evaluation only at the order of $O(1)$, in the case of velocity equation, there exists only an $O(k)$ factor in front of the integral in (39), $P_{\alpha\mu\theta}(\mathbf{k})$. Thus each of the factors, $T^i_{\mu\theta\beta}$ and R^i in (113), should be computed up to the order of $O(k)$. This leads to a significant proliferation of terms in the power-series expansions compared to the case of the temperature equation. Despite the mathematical burden, however, the main techniques employed in this section are similar to those used in the calculation of the effective diffusivities and they will be presented in full details including the main derivations. As a general note, so much details are presented here because these techniques might be directly applicable for similar calculations involving statistical methods for anisotropic turbulence of other physics nature. Transparent but technically difficult calculations are given in Appendixes.

The integrand (113) can be represented as

$$I_{\alpha\beta} = 2Dq^{-3}\sum_{i=1}^{4}\Pi^i_{\alpha\beta}R^i, \quad (114)$$

where

$$\Pi^i_{\alpha\beta} = P_{\alpha\mu\theta}(\mathbf{k})T^i_{\mu\theta\beta}, \quad (115)$$

and, as explained earlier, $\Pi^i_{\alpha\beta}$ and R^i should be calculated up to $O(k^2)$ and $O(k)$, respectively. The $O(k^2)$ expansions of $\Pi^i_{\alpha\beta}$ are very long and not shown here.

Next, calculate the $O(k)$ expansions of the frequency integrals R^i given by Eqs. (106)–(112). Keeping in mind the forthcoming integration over the spherical shell $D^>$, separate the horizontal and vertical terms and represent these expansions as

$$R^i = R^i_0 + k_3q_3R^i_z + k_jq_{hj}R^i_h + O(k^2), \quad (116)$$

where R^i_0, R^i_z, and R^i_h are functions of q and q_3 only; they are given in Appendix B.

C. Integration over the spherical shell $D^>$

Substituting expansion (116) and (114), find

$$I_{\alpha\beta} = 2Dq^{-3}\sum_{i=1}^{4}[(R^i_0+k_3q_3R^i_z)\Pi^i_{\alpha\beta}+k_jq_{hj}R^i_h\Pi^i_{\alpha\beta}]. \quad (117)$$

In this expression, only the factors $\Pi^i_{\alpha\beta}$ and $q_{h_j}\Pi^i_{\alpha\beta}$ depend on the horizontal projection q_{h_j}. Therefore, the shell integral (39) can be written as

$$\begin{aligned}\int_{D^>} I_{\alpha\beta}d^dq &= -\frac{2D\Delta\Lambda}{\Lambda^3}\int_{\Sigma_d}\sum_{i=1}^{4}[(R^i_0+k_3q_3R^i_z)\Pi^i_{\alpha\beta} \\ &\quad + k_jq_{hj}R^i_h\Pi^i_{\alpha\beta}]d^{d-1}q \\ &= -\frac{2D\Delta\Lambda}{\Lambda^2}\sum_{i=1}^{4}\left[\int_0^\pi \Phi^i_{\alpha\beta}(\theta)\right. \\ &\quad \left.\times(R^i_0+k_3q_3R^i_z)d\theta+\int_0^\pi\Psi^i_{\alpha\beta}(\theta)R^i_hd\theta\right],\end{aligned} \quad (118)$$

where the factors

$$\Phi^i_{\alpha\beta} = \int_{\Sigma_{d-1}}\Pi^i_{\alpha\beta}d^{d-2}q = \delta_{\alpha\beta}\Phi_i(k,k_3,\theta), \quad (119)$$

$$\Psi^i_{\alpha\beta} = \int_{\Sigma_{d-1}}k_jq_{hj}\Pi^i_{\alpha\beta}d^{d-2}q = \delta_{\alpha\beta}\Psi_i(k,k_3,\theta) \quad (120)$$

are calculated using decomposition (82) and substitutions $d=3$, $q=\Lambda$, and $P_{33}(\mathbf{q})=\sin^2\theta$ to yield

$$\begin{aligned}\Phi_1(k,k_3,\theta) = \Gamma(\theta)\left[k^2\frac{\cos^2\theta(3+\cos 2\theta)}{4}\right. \\ + k_3^2\frac{\cos^2\theta(1-5\cos 2\theta)}{4} \\ \left. + k_3\Lambda\cos\theta\sin^2\theta\right],\end{aligned} \quad (121)$$

$$\Psi_1(k,k_3,\theta) = \Gamma(\theta)\Lambda^2\left(k^2\frac{\sin^4\theta}{4}-k_3^2\frac{\sin^4\theta}{4}\right), \quad (122)$$

$$\Phi_2(k,k_3,\theta)=\Gamma(\theta)\left[k^2\frac{\cos^2\theta(2+\cos 2\theta)\sin^2\theta}{2}+k_3^2\frac{(-3-4\cos 2\theta-5\cos 4\theta)\sin^2\theta}{8}+k_3\Lambda\cos\theta\sin^4\theta\right], \tag{123}$$

$$\Psi_2(k,k_3,\theta)=\Gamma(\theta)\Lambda^2\left(-k^2\frac{\cos^2\theta\sin^4\theta}{4}+k_3^2\frac{\cos^2\theta\sin^4\theta}{4}\right), \tag{124}$$

$$\Phi_3(k,k_3,\theta)=\Gamma(\theta)\left[k^2\frac{\cos^4\theta\sin^2\theta}{2}+k_3^2\frac{\cos^2\theta(3-5\cos 2\theta)\sin^2\theta}{4}+k_3\Lambda\cos\theta\sin^4\theta\right], \tag{125}$$

$$\Psi_3(k,k_3,\theta)=\Gamma(\theta)\Lambda^2\left(-k^2\frac{\cos^2\theta\sin^4\theta}{4}+k_3^2\frac{\cos^2\theta\sin^4\theta}{4}\right), \tag{126}$$

$$\Phi_4(k,k_3,\theta)=\Gamma(\theta)\left[k^2\cos^4\theta\sin^4\theta-k_3^2\frac{(1+2\cos 2\theta+5\cos 4\theta)\sin^4\theta}{8}+k_3\Lambda\cos\theta\sin^6\theta\right], \tag{127}$$

$$\Psi_4(k,k_3,\theta)=\Gamma(\theta)\Lambda^2\left(-k^2\frac{\cos^2\theta\sin^6\theta}{4}+k_3^2\frac{\cos^2\theta\sin^6\theta}{4}\right), \tag{128}$$

where $\Gamma(\theta)=2\pi\Lambda\sin\theta$. Finally, collecting all the factors, separating the results into groups of terms proportional to k^2 and k_3^2, and taking the limit $\Delta\Lambda\to 0$, obtain a system of two differential equations for ν and ν_z,

$$\frac{d\nu}{d\Lambda}=-\frac{D}{4\pi^3\Lambda^2}\int_0^\pi F(\theta)d\theta, \tag{129}$$

$$\frac{d\nu_z}{d\Lambda}=-\frac{D}{4\pi^3\Lambda^2}\int_0^\pi F_z(\theta)d\theta, \tag{130}$$

where the integrands are

$$F(\theta)=k^{-2}\sum_{i=1}^{4}\left[R_0^i\Phi_i(k,0,\theta)+R_h^i\Psi_i(k,0,\theta)\right], \tag{131}$$

$$F_z(\theta)=F(\theta)+k_3^{-2}\sum_{i=1}^{4}\left[(R_0^i+R_z^i\Lambda\cos\theta)\Phi_i(0,k_3,\theta)+R_h^i\Psi_i(0,k_3,\theta)\right]. \tag{132}$$

In addition to the $O(k_3^2)$ terms, the last expression contains $O(k_3)$ and $O(k_3^3)$ terms under the summation sign. The former terms yield zero contribution to the angular integration in (129) while the latter terms can be neglected as being $O(k_3^3)$ small.

Equations (129), (130), (90), and (91) form a system of four coupled ordinary differential equations for the Λ-dependent effective viscosities and diffusivities,

$$\frac{d\nu}{d\Lambda}=-\frac{D}{2\pi^2\Lambda^5}Q_1(\nu,\nu_z,\kappa,\kappa_z,N/\Lambda^2), \tag{133}$$

$$\frac{d\nu_z}{d\Lambda}=-\frac{D}{2\pi^2\Lambda^5}Q_2(\nu,\nu_z,\kappa,\kappa_z,N/\Lambda^2), \tag{134}$$

$$\frac{d\kappa}{d\Lambda}=-\frac{D}{2\pi^2\Lambda^5}Q_3(\nu,\nu_z,\kappa,\kappa_z,N/\Lambda^2), \tag{135}$$

$$\frac{d\kappa_z}{d\Lambda}=-\frac{D}{2\pi^2\Lambda^5}Q_4(\nu,\nu_z,\kappa,\kappa_z,N/\Lambda^2), \tag{136}$$

where Q_1 through Q_4 are complicated integral expressions that cannot be evaluated analytically. Inspection of these expressions reveals that they are homogeneous functions of order 2, i.e., each one of them can be transformed according to

$$Q(\nu,\nu_z,\kappa,\kappa_z,N/\Lambda^2)=\frac{1}{\nu_n^2}Q\left(\frac{\nu}{\nu_n},\frac{\nu_z}{\nu_n},\frac{\kappa}{\nu_n},\frac{\kappa_z}{\nu_n},\mathcal{F}^{-1}\right), \tag{137}$$

where

$$\mathcal{F}\equiv\frac{\nu_n\Lambda^2}{N} \tag{138}$$

is a spectral Froude number and ν_n is given by Eq. (48). The nondimensionalization with ν_n has been chosen for convenience; either ν or ν_z could also be used. In neutral flows, the eddy viscosity corresponding to the mode Λ determines the eddy turnover time of that mode, $\tau_n=(\nu_n\Lambda^2)^{-1}$. In stably stratified flows, on the other hand, due to anisotropy, the definition of the eddy turnover time is vague and not unique. The ratio of the time scales N^{-1} and τ_n, which is the Froude number $\mathcal{F}$, Eq. (138), characterizes the relative strength of the effects of turbulence and waves in a stably stratified flow. The $\mathcal{F}\to\infty$ and $\mathcal{F}\to 0$ asymptotics describe the cases of weak and strong stratifications, respectively. Furthermore, the scaling with ν_n on the right side of (137) is convenient because it quantifies the deviations of the actual eddy viscosities and eddy diffusivities from their isotropic neutral values. Finally, as will be shown later in Secs. VIII and XII, the definition (138) naturally relates $\mathcal{F}$ to other important characteristics of stably stratified flows.

The full system of equations (133)–(136) cannot be solved analytically and, thus, should be integrated numerically. However, the expansion of the functions Q_1 through Q_4 in powers of $\mathcal{F}^{-1}$ provides an insight into the onset of

flow anisotropization under the action of weak stable stratification. This limit is amenable to analytical exploration and will be considered in Sec. VI.

VI. THE ASYMPTOTIC CASE OF WEAK STABLE STRATIFICATION

Recall that in the case of neutral stratification, Eqs. (133) and (134) reduce to (47) whose solution, $\nu_n(\Lambda)$, is given by Eq. (48), while Eqs. (135) and (136) reduce to the equation for the effective diffusivity of a passive scalar denoted by κ_n whose solution is[18]

$$\left|\frac{\alpha-1.39}{\alpha_0-1.39}\right|^{0.63}\left|\frac{\alpha+2.39}{\alpha_0+2.39}\right|^{0.37}=\frac{\nu_0}{\nu_n}, \tag{139}$$

where $\alpha\equiv Pr_t^{-1}=\kappa_n/\nu_n$, Pr_t is the turbulent Prandtl number, and $\alpha_0=\kappa_0/\nu_0$. In the limit of an infinite Reynolds number corresponding to fully developed turbulence, one finds[18] $Pr_t\simeq 0.72$.

When stable stratification is weak, one can derive the lowest-order approximation to Eqs. (133)–(136) in powers of the small parameter $\mathcal{F}^{-1}$,

$$Q_1=\frac{1}{5\nu_h^2}\left\{1+\mathcal{F}^{-2}\left[\frac{-\nu_h}{14\kappa_h}-\frac{2\kappa_h\nu_h^2}{21(\kappa_h+\nu_h)^3}+\frac{\nu_h^2}{14(\kappa_h+\nu_h)^2}+\frac{\nu_h^2}{14\kappa_h(\kappa_h+\nu_h)}\right]+\frac{\nu_h-\nu_z}{\nu_h}\right\}, \tag{140}$$

$$Q_2=\frac{1}{5\nu_h^2}\left\{1+\mathcal{F}^{-2}\left[\frac{-29\nu_h}{21\kappa_h}+\frac{8\kappa_h\nu_h^2}{21(\kappa_h+\nu_h)^3}-\frac{20\nu_h^2}{21(\kappa_h+\nu_h)^2}+\frac{29\nu_h^2}{21\kappa_h(\kappa_h+\nu_h)}\right]+\frac{2(\nu_h-\nu_z)}{3\nu_h}\right\}, \tag{141}$$

$$Q_3=\frac{2}{3\nu_h(\kappa_h+\nu_h)}\left[1-\frac{\mathcal{F}^{-2}\nu_h}{10\kappa_h}+\frac{2(\kappa_h-\kappa_z)}{5(\kappa_h+\nu_h)}+\frac{2(\kappa_h+2\nu_h)(\nu_h-\nu_z)}{5\nu_h(\kappa_h+\nu_h)}\right], \tag{142}$$

$$Q_4=\frac{2}{3\nu_h(\kappa_h+\nu_h)}\left[1-\frac{4\mathcal{F}^{-2}\nu_h}{5\kappa_h}+\frac{\kappa_h-\kappa_z}{5(\kappa_h+\nu_h)}+\frac{(\kappa_h+2\nu_h)(\nu_h-\nu_z)}{5\nu_h(\kappa_h+\nu_h)}\right]. \tag{143}$$

One can see that the functions Q_1-Q_4 are comprised of $O(1)$ terms corresponding to the case of neutral stratification, small $O(\mathcal{F}^{-2})$ terms, and terms proportional to the differences $(\nu_h-\nu_z)$ and $(\kappa_h-\kappa_z)$. By subtracting Eq. (141) from (140) and Eq. (143) from (142), one can derive differential equations for these differences. Since, at small $\mathcal{F}^{-2}$, these equations can be linearized to become ordinary differential equations (ODEs) with $O(\mathcal{F}^{-2})$ inhomogeneities, their solutions are of the same order, i.e., $\nu_h-\nu_z=O(\mathcal{F}^{-2})$ and $\kappa_h-\kappa_z=O(\mathcal{F}^{-2})$. Therefore, with the exception of the $O(1)$ terms, all terms in Eqs. (140)–(143) are $O(\mathcal{F}^{-2})$ with constant coefficients dependent solely on α. The resulting system of four ODEs can be solved analytically; the solutions are

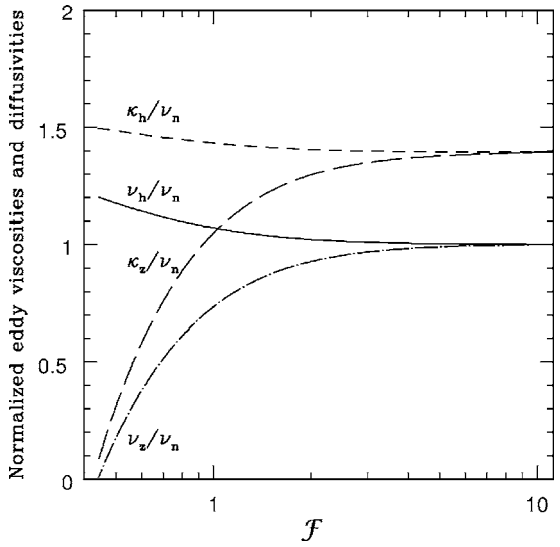

FIG. 1. Large $\mathcal{F}$ asymptotics (weak stratification) of the normalized horizontal and vertical eddy viscosities and diffusivities obtained from the system (133)–(136), (140)–(143).

$$\nu_h/\nu_n=1+0.095\mathcal{F}^{-2}, \tag{144}$$

$$\nu_z/\nu_n=1-0.31\mathcal{F}^{-2}, \tag{145}$$

$$\kappa_h/\nu_n=\alpha+0.054\mathcal{F}^{-2}, \tag{146}$$

$$\kappa_z/\nu_n=\alpha-0.4\mathcal{F}^{-2}. \tag{147}$$

Thus, the normalized horizontal effective viscosity and diffusivity tend to increase with decreasing $\mathcal{F}$ while their vertical counterparts exhibit an opposite tendency pointing to the increasing large-scale anisotropization of the turbulent transport of momentum and heat under the action of stable stratification. Equations (144)–(147) can be used to quantify the onset of this anisotropization; for instance, at $\mathcal{F}\simeq 2$, all effective viscosities and diffusivities differ from their neutral values by less than 10%.

The numerical solution of the nonlinearized asymptotic equations (133)–(136), (140)–(143) is shown in Fig. 1. One can see that for $\mathcal{F}>2$, the effective transport coefficients are close to their neutral values, ν_n and κ_n. When $\mathcal{F}$ decreases below 2, the effective viscosities and diffusivities deviate from ν_n and κ_n significantly; the vertical viscosity and diffusivity decrease while their horizontal counterparts increase. In the transitional range around $\mathcal{F}=1$, the vertical viscosity and diffusivity rapidly decrease with decreasing $\mathcal{F}$ attaining zero values at $\mathcal{F}\simeq 0.4$. At small $\mathcal{F}$, however, the asymptotic equations (140)–(143) are not expected to be valid. The behavior of ν/ν_n, ν_z/ν_n, κ/ν_n, and κ_z/ν_n in the entire range $\mathcal{F}>0$ can be investigated by solving the full system (133)–(136) numerically; this solution is shown in Fig. 2. For relatively weak stratification, $\mathcal{F}>1$, the asymptotic and full solutions are in good agreement. In the limit of strong stable stratification, $\mathcal{F}\to 0$, turbulence anisotropization is reflected in the pronounced disparity between the horizontal and vertical viscosities and diffusivities. Unlike the asymptotic so-

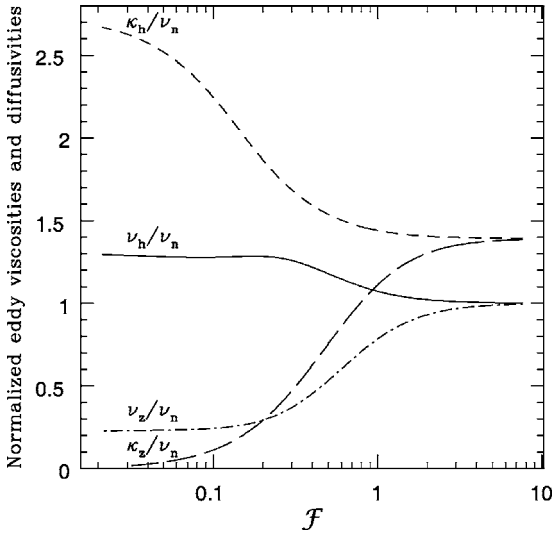

FIG. 2. Normalized horizontal and vertical eddy viscosities and diffusivities as functions of $\mathcal{F}$ obtained from the full system (133)–(136).

lution that attains zero values at $\mathcal{F}\simeq 0.4$, in the full solution, the effective viscosities and diffusivities are always positive.

The asymptotic expansions of the functions Q_1-Q_4 for the case of strong stratification are given in Appendix C.

Finally, it should be emphasized that the spectral-space Eqs. (133)–(136) have been obtained strictly within the QNSE model with no additional approximations or closures. For practical applications, one needs to relate the forcing amplitude D to observable parameters. This can be done by using an energy balance equation as elaborated in Sec. VII.

VII. THE FORCING AMPLITUDE *D*

Determine the forcing amplitude D in (34) in the neutral case. The Green function $G_{\alpha\beta}$ becomes a diagonal isotropic tensor $G_{\alpha\beta}(\omega,\mathbf{k})=[-i\omega+\nu(k)k^2]\delta_{\alpha\beta}$. Recall that one of the main points of the distant interaction approximation is the identification of the damping parameter $\nu(k)$ in the Green function with the effective viscosity $\nu_n(\Lambda)$ at $\Lambda=k$ yielding

$$G_{\alpha\beta}(\omega,\mathbf{k})=[-i\omega+\nu_n(k)k^2]\delta_{\alpha\beta}. \tag{148}$$

Using this representation together with Eqs. (36) and (48), calculate the three-dimensional (3D) energy spectrum,

$$E(k)=(2\pi)^{-3}k^2\int U_{\alpha\alpha}(k,\omega)d\omega=0.26D^{2/3}k^{-5/3}. \tag{149}$$

The expression for D is derived from the energy dissipation equation,

$$\epsilon=2\nu_n(\Lambda)\int_0^\Lambda p^2E(p)dp. \tag{150}$$

This equation emphasizes the energy loss by the slow modes $0<k<\Lambda$ due to the action of the effective viscosity $\nu_n(\Lambda)$ accumulated as a result of elimination of the fast modes $k>\Lambda$. Substituting Eqs. (48) and (149) in (150), find

$$D\simeq 13.1\epsilon. \tag{151}$$

This equation can be used to represent the effective viscosity and the energy spectrum of homogeneous isotropic turbulence in the neutral case, Eqs. (48) and (149), in terms of the dissipation rate ϵ,

$$\nu_n(\Lambda)\simeq 0.46\epsilon^{1/3}\Lambda^{-4/3}, \tag{152}$$

$$E_0(k)=C_K\epsilon^{2/3}k^{-5/3}, \tag{153}$$

where the Kolmogorov constant $C_K\simeq 1.45$. It should be noted that the latter derivation is in the spirit of a derivation given in Ref. 31. Using a different closure relating ϵ and D based on Eq. (31), the authors of Ref. 31 derived an expression for the energy flux through a mode k, equated it to the energy dissipation rate and found $D\simeq 15.7\epsilon$ leading to $C_K\simeq 1.6$. Both this and our value $C_K\simeq 1.45$ agree well with the estimate,

$$C_K=1.5\pm 0.15, \tag{154}$$

obtained in high Reynolds number flows.[32]

The assumption of the forcing isotropy, quite natural for neutrally stratified, isotropic turbulence, may be violated for modeling flows with stable stratification. However, it is asymptotically valid for diminishing stratification and should hold in the limit of large k where the effect of stratification decreases. As an approximation, this assumption will be adopted in this study and extrapolated to the range of small k where the stratification effect is strong. This approach makes it possible to explore the limits of validity of the approximation of isotropic forcing. Note that this approximation by no means precludes the system from developing anisotropic features due to stable stratification. The anisotropization is reflected in the velocity and temperature Green functions, $G_{\alpha\beta}(\omega,k,k_3)$ and $G_T(\omega,k,k_3)$, as well as in the auxiliary Green function $G(\omega,k,k_3)$.

VIII. THE OZMIDOV LENGTH SCALE

Taking into account Eq. (152), the spectral Froude number $\mathcal{F}$ can be represented as

$$\mathcal{F}=\frac{\nu_n(k)k^2}{N}\approx 0.5\left(\frac{k}{k_O}\right)^{2/3}, \tag{155}$$

where

$$k_O=\left(\frac{N^3}{\epsilon}\right)^{1/2} \tag{156}$$

is the Ozmidov wave number. Similar to $\mathcal{F}$, the ratio k/k_O can be used as a nondimensional parameter characterizing the strength of stratification. The cases of weak and strong stratifications are recovered in the limits $k/k_O\to\infty$ and $k/k_O\to 0$, respectively. The asymptotic equations for the former case, Eqs. (144)–(147), can be recast in a form directly exposing the dependence of the effective viscosities and diffusivities on the ratio k/k_O,

$$\nu_h/\nu_n=1+0.38(k/k_O)^{-4/3}, \tag{157}$$

$$\nu_z/\nu_n=1-1.24(k/k_O)^{-4/3}, \tag{158}$$

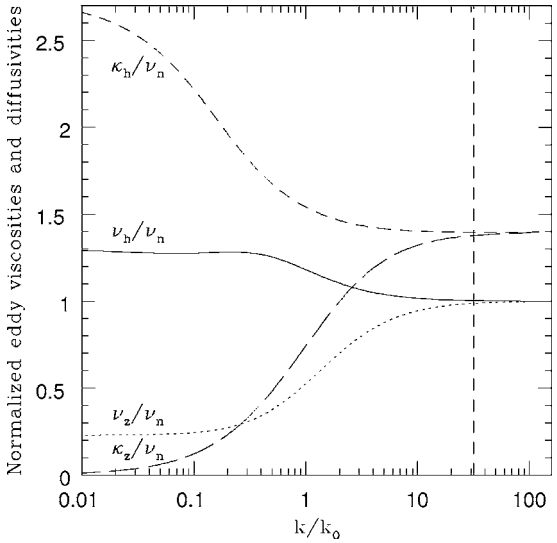

FIG. 3. Normalized horizontal and vertical eddy viscosities and diffusivities as functions of k/k_O. The dashed vertical line shows the threshold of internal wave generation in the presence of turbulence.

$$\kappa_h/\nu_n = \alpha + 0.22(k/k_O)^{-4/3}, \tag{159}$$

$$\kappa_z/\nu_n = \alpha - 1.6(k/k_O)^{-4/3}. \tag{160}$$

The Ozmidov wave number provides important characterization of the effect of stable stratification also from the viewpoint of temporal scales. Let us recall the classical dispersion relation for linear internal waves,[33]

$$\omega_0^2 = N^2 \sin^2\theta. \tag{161}$$

Equating the characteristic time scale for the linear waves, $(N|\sin\theta|)^{-1}$, and the turnover time scale for an eddy of the size k^{-1}, given by $[k^3E(k)]^{-1/2}$, $E(k)$ being the Kolmogorov spectrum (153), obtain a characteristic wave number of the internal wave-turbulence transition,

$$k_{\mathrm{wt}} \simeq k_O|\sin\theta|^{3/2}. \tag{162}$$

Full solutions for the normalized effective viscosities and diffusivities, ν_h/ν_n, ν_z/ν_n, κ_h/ν_n, and κ_z/ν_n, are presented in Fig. 3 as functions of k/k_O. At large k/k_O (small scales), as expected, all the parameters approach their corresponding isotropic values. At small k/k_O, on the other hand, horizontal and vertical viscosities and diffusivities depart markedly. The horizontal viscosity increases by a factor of 1.3 compared to the neutral case, while the vertical viscosity decreases to approximately 0.15 of the horizontal viscosity value. Even for very strong stable stratification, on scales for which $k/k_O \ll 1$, ν_z seems to preserve a finite asymptotic value that is larger than the molecular viscosity. Another interesting result is that $\kappa_z/\kappa_h \to 0$ for $k/k_O \to 0$, i.e., under strong stratification, vertical diffusivity is suppressed while its horizontal counterpart is enhanced increasing by about a factor of 2 over its value in the neutral case.

IX. DISPERSION RELATION FOR INTERNAL WAVES IN THE PRESENCE OF TURBULENCE AND INTERNAL WAVE FREQUENCY SHIFT

An approach based upon the Langevin equations provides a convenient framework for characterization of nonlinear waves. Indeed, write the Langevin equation (31) as

$$G^{-1}_{\alpha\beta}(\omega,\mathbf{k})u_\beta(\omega,\mathbf{k}) = f_\alpha(\omega,\mathbf{k}). \tag{163}$$

This equation describes linear, forced, stochastic oscillator whose eigenfrequencies are given by the secular equation,

$$\det[G^{-1}_{\alpha\beta}(\omega,\mathbf{k})] = 0. \tag{164}$$

Straightforward calculation yields a solution to Eq. (164),

$$\omega_{1,2} = -\frac{i}{2}(\omega_q + \omega_q^T) \pm \frac{1}{2}\sqrt{4N^2P_{33}(\mathbf{q}) - (\omega_q - \omega_q^T)^2}, \tag{165}$$

which describes decaying in time waves. The frequencies of these waves are given by the real part of (165),

$$\omega = \omega_0\left(1 - \mathcal{F}^2\left\{\frac{[(\kappa_z/\nu_n) - (\nu_z/\nu_n)]\cos^2\theta + [(\kappa_h/\nu_n) - (\nu_h/\nu_n)]\sin^2\theta}{2\sin\theta}\right\}^2\right)^{1/2}, \tag{166}$$

or, in terms of the ratio k/k_O,

$$\omega = \omega_0\left(1 - \left(\frac{k}{k_O}\right)^{4/3}\left\{\frac{[(\kappa_z/\nu_n) - (\nu_z/\nu_n)]\cos^2\theta + [(\kappa_h/\nu_n) - (\nu_h/\nu_n)]\sin^2\theta}{4\sin\theta}\right\}^2\right)^{1/2}, \tag{167}$$

where ω_0 is given by (161). Equations (166) and (167) are, in fact, dispersion relations for internal waves in the presence of turbulence; they quantify the internal wave frequency shift due to turbulence. In the limit of $\mathcal{F} \to 0$ or $k/k_O \to 0$ (strong stratification), the classical dispersion relation for linear internal waves is recovered. Note that $\omega \leqslant \omega_0 \leqslant N$ for any stratification which is consistent with the observations of flows with internal waves.[34,35] Note also that Eqs. (166) and

(167) are the real part of the poles $\Omega_{6,7,8,9}$ given by Eq. (110); they account for internal wave contribution to effective viscosities and diffusivities.

X. THE THRESHOLDS OF INTERNAL WAVE GENERATION

The omega functions given by Eqs. (166) and (167) decrease with increasing $\mathcal{F}$ or k/k_O and become zero at some k. This can be interpreted as an indication of increasingly disorganizing action of the turbulent overturn that negates the selective ordering between ω and k characteristic of internal waves. The threshold value $\omega=0$ selects a scale at which turbulent scrambling begins to overwhelm internal wave generation. The corresponding Froude number (referred to as the critical Froude number $\mathcal{F}_{\text{crit}}$) can be associated with the threshold of internal wave generation in the presence of turbulence,

$$\mathcal{F}_{\text{crit}} = \left| \frac{2 \sin\theta}{[(\kappa_z/\nu_n) - (\nu_z/\nu_n)]\cos^2\theta + [(\kappa_h/\nu_n) - (\nu_h/\nu_n)]\sin^2\theta} \right|. \tag{168}$$

The same criterion can be rewritten in terms of the critical wave number k_t:

$$k_t = k_O \left| \frac{4 \sin\theta}{[(\kappa_z/\nu_n)] - [(\nu_z/\nu_n)]\cos^2\theta + [(\kappa_h/\nu_n)] - [(\nu_h/\nu_n)]\sin^2\theta} \right|^{3/2}. \tag{169}$$

Assuming that the wave radiation begins at relatively large k, while turbulence is still close to isotropic, and using Eqs. (144)–(147) to estimate $\kappa_z/\nu_n - \nu_z/\nu_n \approx 0.4$ and $\kappa_h/\nu_n - \nu_h/\nu_n \approx 0.4$ in this limit, find from Eq. (168) that

$$\mathcal{F}_{\text{crit}} \simeq 5|\sin\theta| \leqslant 5. \tag{170}$$

Thus, $\mathcal{F}_{\text{crit}}=5$ can be used as a threshold criterion of internal waves generation in the presence of turbulence in the sense that the waves can only exist for $\mathcal{F} \leqslant \mathcal{F}_{\text{crit}}$. Comparing this criterion with Eqs. (144)–(147) one concludes that internal wave generation and flow field anisotropization commence at approximately the same scales.

Another threshold criterion of internal waves generation can be derived from Eq. (169),

$$k_t \simeq k_O|10 \sin\theta|^{3/2} \simeq 32 k_O|\sin\theta|^{3/2}. \tag{171}$$

Internal waves can only exist for the wave vectors defined by the interior of the torus $k \leqslant k_t$ shown in Fig. 4. The maximum threshold wave number of internal wave generation is attained along the directions $\theta = \pm\pi/2$ where it is equal to $32k_O$. This value of the threshold is shown in Fig. 3 as a vertical dashed line. At this value of k_t, turbulent viscosities and diffusivities just begin to deviate from their values under neutral stratification thus providing *a posteriori* justification to the use of neutral case viscosities and diffusivities made to derive Eq. (171). Only when $\theta \to 0$ or $\theta \to \pi$, k_t becomes small requiring more precise technique of solving Eq. (169). Note that the toroidal surface described by (171) is, in fact, the same as that given by (162) with the exception of the coefficient 32 in the former versus 1 in the latter.

XI. TURBULENCE SPECTRA

Since the structure of stably stratified flows is strongly anisotropic, traditional 3D energy spectrum (149) provides only limited characterization of the flow field. Various one-dimensional (1D) spectra of the vector field $\mathbf{u}(\mathbf{x})$ give far more detailed information in this case.[36] These spectra are obtained by integration of the diagonal components of the spectrum tensor $U_{\alpha\beta}(\omega, \mathbf{k})$ over planes enclosing the axis k_α or orthogonal to it {and yielding transversal $[E_\alpha(k_\beta),\ \alpha \neq \beta]$ and longitudinal $[E_\alpha(k_\alpha)]$ spectra, respectively}. Such spectra provide diagnostics of the energy redistribution among different components due to the action of stable stratification. Taking into account the horizontal isotropy of the velocity field note that there exist only five nontrivial 1D spectra: (a) the energy spectrum of a horizontal velocity component, say, u_1, as a function of the vertical wave number, $E_1(k_3)$; (b) the energy spectrum of a horizontal velocity component u_1 as a function of the horizontal wave number k_1, $E_1(k_1)$; (c) the energy spectrum of a horizontal velocity component as a function of the horizontal wave number orthogonal to k_1, $E_1(k_2)$; (d) the energy spectrum of the vertical velocity com-

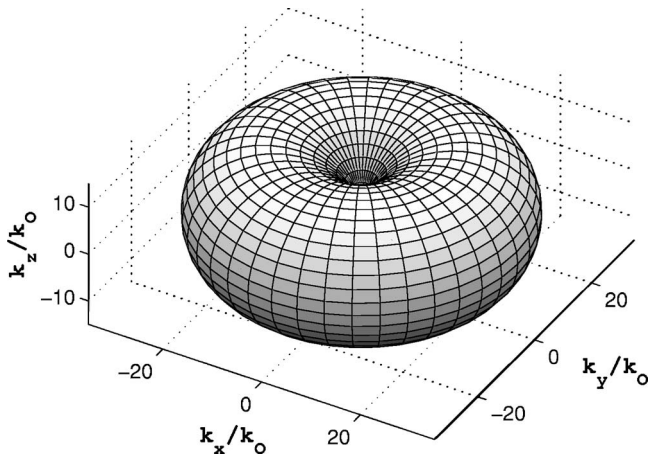

FIG. 4. The torus given by Eq. (171) defines the threshold of internal wave generation in the presence of turbulence: admissible wave vectors must belong to the torus interior.

ponent as a function of the horizontal wave number, $E_3(k_1)$; and (e) the energy spectrum of the vertical velocity component as a function of the vertical wave number, $E_3(k_3)$. The most interesting 1D characteristics are (a), (d), and (e). These spectra have been discussed in the literature and there exist some data available for comparisons with QNSE model predictions. At the end of the section, the 3D energy spectrum will also be considered as it has important applications in the Reynolds-averaged Navier-Stokes (RANS) modeling discussed in Sec. XII. Let us make a general remark that very often the 1D spectra found in observations and simulations are cast in terms of k rather than the corresponding components k_α which may lead to confusion in some situations.[24] Although the spectra below will be given in terms of k_α, in comparison with the data and simulations, the difference between k and k_α will not be accentuated because rigorous dependence on k_α is often unavailable.

A. The spectrum $E_1(k_3)$

The 1D spectrum $E_1(k_3)$ is calculated according to

$$E_1(k_3) = \frac{4}{\pi}\int_{-\infty}^{\infty}\frac{d\omega}{2\pi}\int_0^\infty\int_0^\infty \frac{dk_1dk_2}{(2\pi)^2}U_{11}(\omega,\mathbf{k}). \tag{172}$$

Generally, this integral is computed numerically, first, by frequency integration using contour methods and then integration over the plane k_2k_3. However, in the case of weak stratification, using Eqs. (144)–(147), the integration can be carried out analytically yielding

$$E_1(k_3) = 0.626\epsilon^{2/3}k_3^{-5/3} + 0.214N^2k_3^{-3}. \tag{173}$$

This result has several important implications. First, the coefficient with the neutral transverse spectrum, 0.626, is in a very good agreement with the corresponding value of 0.62 given in Ref. 36 thus providing an additional validation of the QNSE model. Second, the addition to that spectrum due to stable stratification is proportional to $N^2k_3^{-3}$; the result that has been widely discussed in the literature.[37–41] Note that in the previous discussions, this term was expressed in terms of k rather than k_3 although the latter has a more rigorous meaning. The value of the coefficient in front of this term was estimated in LES (Ref. 41) as 0.2; it is in a very good agreement with the value 0.214 found here analytically.

B. The spectrum $E_3(k_1)$

The 1D spectrum $E_3(k_1)$ is calculated according to

$$E_3(k_1) = \frac{4}{\pi}\int_{-\infty}^{\infty}\frac{d\omega}{2\pi}\int_0^\infty\int_0^\infty \frac{dk_2dk_3}{(2\pi)^2}U_{33}(\omega,\mathbf{k}). \tag{174}$$

Again, in the general case, this integral can be computed numerically. However, in the case of weak stratification, an analytical evaluation of (174) is possible yielding

$$E_3(k_1) = 0.626\epsilon^{2/3}k_1^{-5/3} - 0.704N^2k_1^{-3}. \tag{175}$$

Based upon the rapid distortion theory of turbulence, a similar expression was derived in Ref. 42 with an $O(1)$ coefficient in front of $N^2k_1^{-3}$. The analytically derived Eq. (175) confirms this result and provides the value of that coefficient.

C. The spectrum $E_3(k_3)$

The 1D spectrum $E_3(k_3)$ is calculated according to

$$E_3(k_3) = \frac{4}{\pi}\int_{-\infty}^{\infty}\frac{d\omega}{2\pi}\int_0^\infty\int_0^\infty \frac{dk_1dk_2}{(2\pi)^2}U_{33}(\omega,\mathbf{k}). \tag{176}$$

As in the previous two cases, the integration in (176) can be performed numerically. An analytical integration is possible in the case of weak stratification yielding

$$E_3(k_3) = 0.47\epsilon^{2/3}k_3^{-5/3} - 0.143N^2k_3^{-3}. \tag{177}$$

Take a note that the coefficient 0.47 for the neutral longitudinal spectrum is in very good agreement with the corresponding value of 0.46 given in Ref. 36. Note also that if Eq. (173) suggests that there is a transition from the $-5/3$ to -3 spectrum at small k/k_O, the other two spectra, (175) and (177), only indicate that the corresponding Kolmogorov spectra decrease with increasing stratification. It is important to keep in mind that asymptotic equations (173), (175), and (177) are only valid in the case of weak stratification and weak anisotropy. In order to obtain comprehensive expressions for the 1D spectra valid for small k/k_O, one needs to perform numerical integration in Eqs. (172), (174), and (176) using full solution of the system (133)–(136). Such calculated spectra always remain positive.

The other two 1D spectra mentioned earlier in this section are modified by stratification only slightly such that the horizontal spectrum as a function of the horizontal wave number remains close to the $-5/3$ scaling law which is in agreement with recent simulations by Lindborg.[43] More detailed comparisons with various experimental, observational, and simulated spectra are beyond the scope of this paper and will be reported elsewhere.

D. Three-dimensional energy spectrum

The 3D energy spectrum can be calculated from the spectrum tensor (60) according to

$$E(k) = \frac{1}{2}k^2\int_{-\infty}^{\infty}\frac{d\omega}{2\pi}\int_{\partial S_3}\frac{d\Sigma}{(2\pi)^3}U_{\alpha\alpha}(\omega,\mathbf{k}), \tag{178}$$

where $\int_{\partial S_3}d\Sigma$ denotes integration over the surface of a three-dimensional unit sphere and the summation rule is imposed. This integration was performed using contour methods for the frequency integration and standard analytical methods for the angular integration; the resulting total energy spectrum is shown in Fig. 5. One observes that at the same dissipation rate, the spectrum of a stably stratified flow is very close to the classical Kolmogorov spectrum (153) of a neutral flow. The deviation between the spectra is confined to the range $k<k_O$ where the spectrum of stratified flows becomes somewhat smaller than the Kolmogorov spectrum.

Summarizing the results of this section, let us reiterate that the present model reveals spectral anisotropization caused by stable stratification. This anisotropization manifests itself as energy increase in the horizontal velocity components at the expense of their vertical counterpart. However, despite considerable energy redistribution among various velocity components, the 3D energy spectrum re-

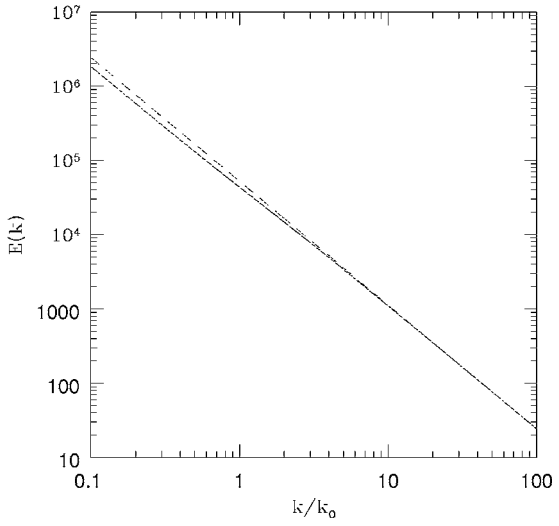

FIG. 5. The total energy spectrum. The dashed line shows the classical Kolmogorov $-5/3$ spectrum (153) for the case of neutral stratification. The solid line shows the total spectrum of a stably stratified flow.

mains close to the classical Kolmogorov spectrum. Although, as will be shown in Sec. XII, this property of the 3D spectrum is useful for derivation of the RANS models, it obscures the physics of the effect of stable stratification. In strongly anisotropic flows, such as stratified and/or rotating flows, consideration of a variety of 1D spectra is essential.[24] Note in this respect that in stably stratified flows, only the horizontal spectrum, $E_1(k_3)$, has been studied relatively well. For better understanding of the physics of stably stratified flows and for comprehensive validation of theoretical models, it is essential to obtain experimental and computational information for other 1D spectra.

XII. QNSE-BASED RANS MODELS AND THEIR VALIDATION

A. Transport coefficients in the RANS format

In this section, it will be shown how the QNSE model developed above can be used for practical simulations of turbulent flows with stable stratification. The process of small-scale elimination is now extended to the largest scales of the system where turbulence still exists, i.e., to the integral length scale k_L^{-1}. This approach is analogous to the Reynolds averaging procedure and the resulting equations comprise a RANS model. In this context, the effective viscosities and diffusivities will be identified with the *eddy* viscosities and diffusivities.

In Sec. XI it was shown that the 3D energy spectrum of stably stratified flows does not significantly depart from the Kolmogorov distribution (153) and, thus, can be used to calculate the total energy of the flow field,

$$K = \int_{k_L}^{\infty} C_K \epsilon^{2/3} k^{-5/3} dk \simeq 2.2 \epsilon^{2/3} k_L^{-2/3}, \tag{179}$$

from which

$$\frac{K^2}{\epsilon} = 2.2^2 \epsilon^{1/3} k_L^{-4/3}. \tag{180}$$

Comparing this with the equation for the eddy viscosity in neutral flows, Eq. (152), find

$$\nu_n = C_\mu^0 \frac{K^2}{\epsilon}, \tag{181}$$

where $C_\mu^0 \simeq 0.095$, which is a well-known result from K-ϵ modeling.

The spectral Froude number $\mathcal{F}$ defined in (138) can be adopted for the RANS modeling if k is replaced by k_L. Denoting the RANS Froude number as Fr and evaluating it using Eqs. (180) and (181), find

$$\mathrm{Fr} = \frac{\nu_n k_L^2}{N} \simeq \frac{\epsilon}{KN}, \tag{182}$$

i.e., Fr is the same Froude number as the one used in Refs. 44 and 45. The use of Fr for characterization of the effects of stratification in turbulent flows is convenient because Fr is well defined in both shear and shear-free flows. Also, as found in Ref. 45 Fr is a parameter giving better correlations with various data than other parameters.

Note that the behavior of the energy spectrum in the vicinity of k_L is relatively uncertain and nonuniversal, so that Eq. (179) is approximate within an $O(1)$ factor which itself may depend on other parameters, for instance, the mean shear. For these reasons, Eq. (182) is also approximate within an $O(1)$ factor. This factor can be estimated via calibration against observational, laboratory or DNS data. However, no such calibration was performed here. The QNSE-based RANS model results will be compared with DNS database developed in Ref. 44; the initial Taylor microscale Reynolds number was about 90.

Using (181), obtain an expression for the vertical eddy viscosity in stratified flows,

$$\nu_z = C_\mu(\mathrm{Fr}) \frac{K^2}{\epsilon}, \tag{183}$$

where

$$C_\mu(\mathrm{Fr}) = C_\mu^0 \frac{\nu_z}{\nu_n} \tag{184}$$

is a Fr-dependent coefficient sometimes referred to as the eddy viscosity parameter.[45] Figure 6 compares Eq. (184) with the DNS data from Refs. 44 and 45. The agreement is good for $\mathrm{Fr} > 0.3$; for stronger stratification and smaller Fr, turbulence in DNS was suppressed, possibly, due to the low Reynolds number.

Figure 7 compares the normalized vertical viscosity and diffusivity, ν_z/ν_n and κ_z/ν_n, obtained in the QNSE model with those simulated in DNS.[44] Although the data show a considerable spread, there exists a relatively good general and quantitative agreement between the QNSE model and the DNS data for $\mathrm{Fr} > 0.3$. At smaller Fr, turbulence was suppressed in DNS. As explained earlier, the agreement could be somewhat improved with a proper calibration of

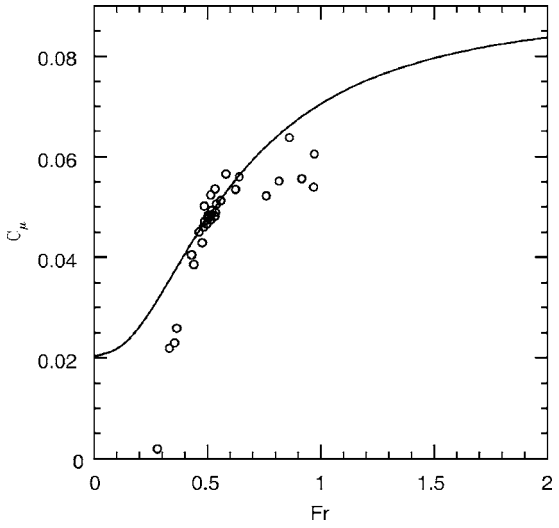

FIG. 6. The eddy viscosity parameter C_μ as a function of the Froude number Fr. The circles show the DNS data from Refs. 44 and 45; solid line is Eq. (184).

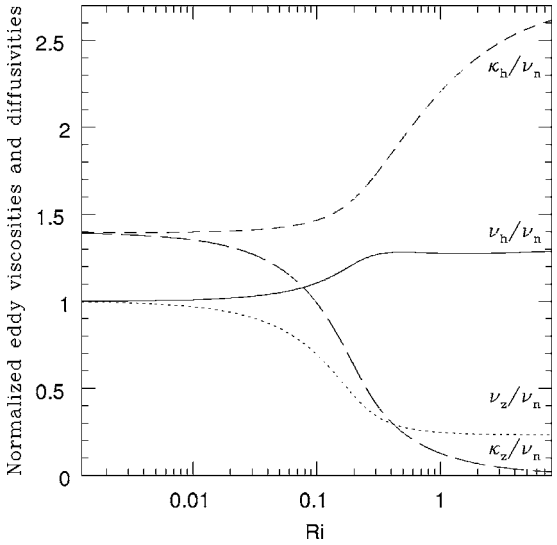

FIG. 8. Normalized eddy viscosities and diffusivities as functions of the gradient Richardson number Ri.

Eq. (179). However, since the Reynolds number in DNS was low and the amount of data was limited, such a calibration is deemed unwarranted at this time.

Stratified turbulent shear flows are often characterized by the gradient Richardson number $\mathrm{Ri}=N^2/S^2$, where S is the magnitude of the shear. Since the mean shear was not included in the QNSE model, an additional closure assumption is required to bring S into consideration. For such an assumption, a balance between the rate of the energy dissipation, ϵ, the shear production $P=\nu_z S^2$, and the buoyancy destruction $B=\kappa_z N^2$ is chosen,

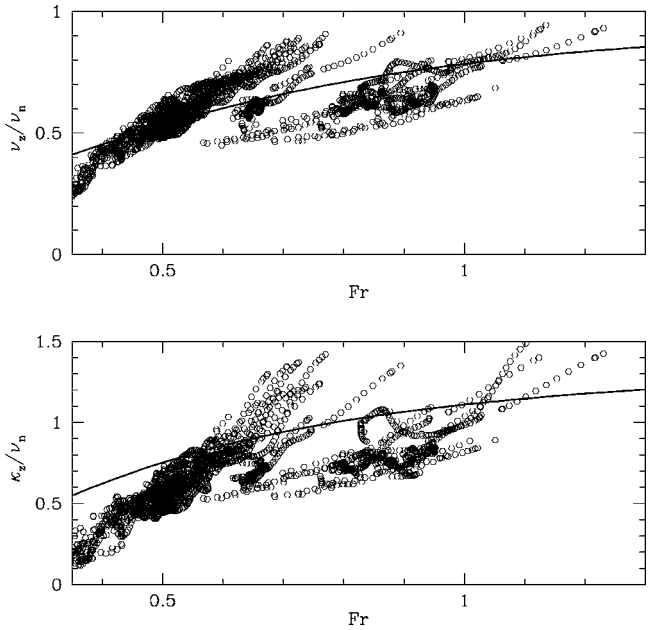

FIG. 7. The nondimensional vertical eddy viscosity (top) and eddy diffusivity (bottom) as functions of the Froude number Fr. The circles show the DNS data from Ref. 44; the solid line is QNSE model.

$$\epsilon = P - B = \nu_z S^2 - \kappa_z N^2 = \nu_z S^2 (1 - \mathrm{Ri}/\mathrm{Pr}_t), \tag{185}$$

where $\mathrm{Pr}_t=\nu_z/\kappa_z$ is the "vertical" turbulent Prandtl number, Pr_t. This assumption focuses the RANS model on flows close to local equilibrium. Such flows are abundant in the atmosphere and the oceans and many models used in geophysical applications also assume local equilibrium or small deviations from it.[46] Therefore, using the assumption (185), the present model can be applied to and validated in a wide variety of geophysical flows. In addition, by testing the model in strongly nonequilibrium flows it may be possible to establish the limits of its applicability and to find simple adjustments that may extend the limits of model's applicability.

Equations (152) and (185) enable one to relate Ri to the parameters of the RANS model. Using (152) find

$$\nu_n \simeq 0.5 \epsilon^{1/3} k_L^{-4/3}. \tag{186}$$

Substitution of (185) in (186) yields

$$\nu_n = 0.5 S^{2/3} [(1 - \mathrm{Ri}/\mathrm{Pr}_t)\nu_z]^{1/3} k_L^{-4/3}, \tag{187}$$

from which

$$\nu_n k_L^2 = 0.5^{3/2} [(1 - \mathrm{Ri}/\mathrm{Pr}_t)]^{1/2} \left(\frac{\nu_z}{\nu_n}\right)^{1/2} S. \tag{188}$$

Using the definition of Fr, Eq. (182), and Eq. (188), find

$$\mathrm{Ri} = \frac{c_\nu \mathrm{Pr}_t}{c_\nu + \mathrm{Fr}^2 \mathrm{Pr}_t (\nu_n/\nu_z)}, \tag{189}$$

where $c_\nu=0.125$. Using (189), the normalized eddy viscosities and diffusivities, ν_h/ν_n, ν_z/ν_n, κ_h/ν_n, and κ_z/ν_n, can be presented as functions of Ri; see Fig. 8. The eddy viscosities and diffusivities begin to depart from their neutral values at relatively small Ri. The most significant change in their behavior takes place in the range of Ri between 0.1 and 1 in which the vertical mixing of momentum and temperature is suppressed while the horizontal mixing is enhanced. These results do not support the existence of a single valued Ri at

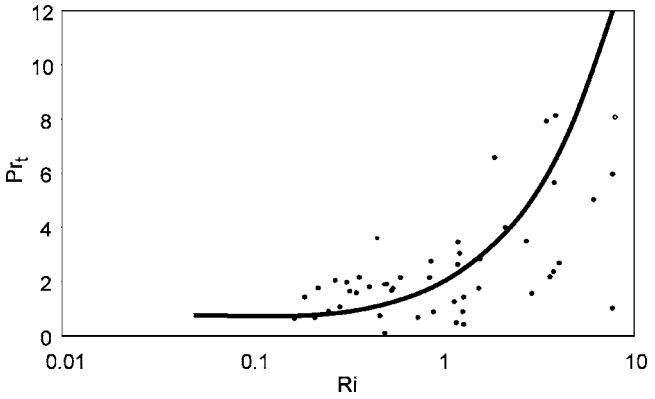

FIG. 9. Turbulent Prandtl number as a function of the gradient Richardson number Ri. The dots are the experimental data from Huq and Stewart (Huq, 2004, private communication); the solid line shows the present model's results.

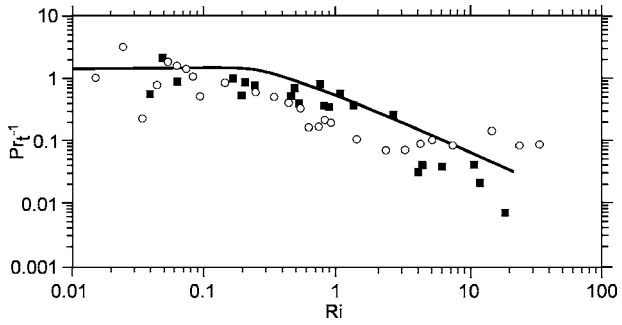

FIG. 10. Inverse vertical turbulent Prandtl number, Pr_t^{-1}, as a function of Ri. The black squares are the experimental data from Ref. 50; the open circles are the field data from Ref. 51; the solid line is obtained from the present RANS model.

which turbulence is abruptly suppressed; rather, they are consistent with the discussion of DNS results in Ref. 45 which also noted the gradual nature of turbulence-internal wave transition. Furthermore, these results are consistent with the abundant volume of the data collected in meteorological and oceanographic observations in which turbulence existed in flows with Ri far exceeding the critical value of 0.25 (Refs. 47 and 48) and 1 (Ref. 49) (also see Refs. 50–53).

For $\mathrm{Ri}>0.1$, both the vertical eddy viscosity and diffusivity decrease: ν_z falls to about one-third of its neutral value while κ_z decreases much faster than ν_z. Eventually, stable stratification completely suppresses vertical scalar mixing while vertical momentum mixing continues even at relatively high Ri. The tendency of the effective vertical viscosity to attain constant values and even to increase with increasing Ri has been revealed in recent observations[51] and high-resolution simulations[52,54] where it was attributed to the momentum mixing by internal waves.[55,56] This mixing has also been detected in oceanic observations which consistently reveal significant levels of turbulence inside and underneath a strong thermocline.[57–59] Such behavior is not easily reproducible in RANS models or in second-moment closure models which both exclude internal waves. In the context of physical oceanography, the concept of externally imposed "residual" or "background" mixing has been routinely utilized to supplement the Reynolds stress closure-predicted mixing to account for turbulence that survives at Ri beyond the critical Richardson number.[57,60]

The behavior of the vertical turbulent Prandtl number $\mathrm{Pr}_t=\nu_z/\kappa_z$ is of great practical importance because it characterizes the relative diffusion of momentum and heat. Figure 9 compares prediction of the present model with the experimental data from Huq and Stewart (Huq, 2004, private communication). Both the data and the model indicate that Pr_t increases with increasing Ri in the entire range of available Richardson numbers from 0.1 to 10; the data and the model are in good quantitative agreement.

Another comparison of the theoretical prediction, this time for Pr_t^{-1}, with the data collected in recent experiments[50] and field observations[51] is shown in Fig. 10. Again, the general trend of Pr_t^{-1} is reproduced well and the quantitative agreement between the data and the model is good. A similar behavior of either Pr_t or Pr_t^{-1} was also found in earlier field observations of the atmospheric boundary layers[61] and recent high-resolution simulations for $\mathrm{Ri}<2$.[52]

In summary, the results of this section demonstrate that when used in the RANS mode, the QNSE model produces the vertical eddy viscosity and eddy diffusivity in good agreement with laboratory and observational data and DNS. This is an important prerequisite for successful application of the QNSE model for accurate simulation of practically important flows. Section XII B briefly describes testing of these eddy viscosity and eddy diffusivity in simulations of the atmospheric boundary layer over sea ice.

B. Numerical test: *K*-ϵ-based simulations of the atmospheric boundary layer over sea ice

Here we present a condensed discussion of how the theoretically derived eddy viscosity and eddy diffusivity perform when implemented in a *K*-ϵ model and used to simulate a stably stratified atmospheric boundary layer. Full account of these simulations is given elsewhere.[62]

The QNSE-RANS model implemented in the *K*-ϵ format was tested in the single-column (time- and vertical coordinate-dependent) simulations of the stably stratified atmospheric boundary layer (SBL) over sea ice in a test case involving the Beaufort Arctic Storms Experiment (BASE). These data has been faithfully reproduced in LES (Ref. 63) which, thus, can be used as a benchmark. The data were available for the cases of moderate and strong stable stratifications so that the model could be tested in both situations. The difference between these cases was in the rate of surface cooling equal to 0.25° K h^{-1} in the former and 1.0° K h^{-1} in the latter. The strength of the overlying inversion was 0.01° K m^{-1} and the surface roughness was 0.1 m. As a carrier of the present *K*-ϵ model, a 1D version of a regional weather forecast model[64,65] has been used. In its *K*-ϵ engine, the QNSE-derived eddy viscosity and eddy diffusivity have been implemented. In addition, the dissipation equation incorporated a correction that accounts for the effect of the planetary rotation[66] and an analogous correction that accommodates the effect of stratification.[62] Even with all these new features, RANS is much less computationally expensive than full LES and therefore it is important to check whether or not

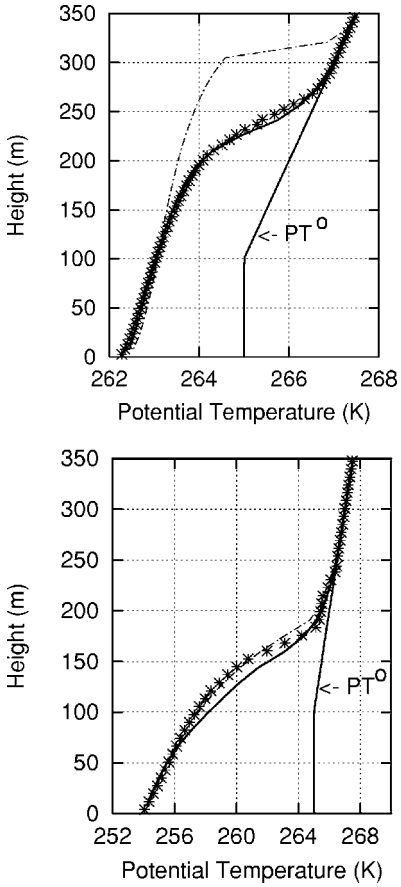

FIG. 11. Vertical profiles of mean potential temperature for the cases of moderate (top panel) and strong (bottom panel) stable stratification simulated with the new (solid line) and the standard (dashed-dotted line) K-ϵ models. The LES results (Ref. 63) are shown by the asterisks. The initial PT profiles (marked as PT^0) are shown by the straight solid lines.

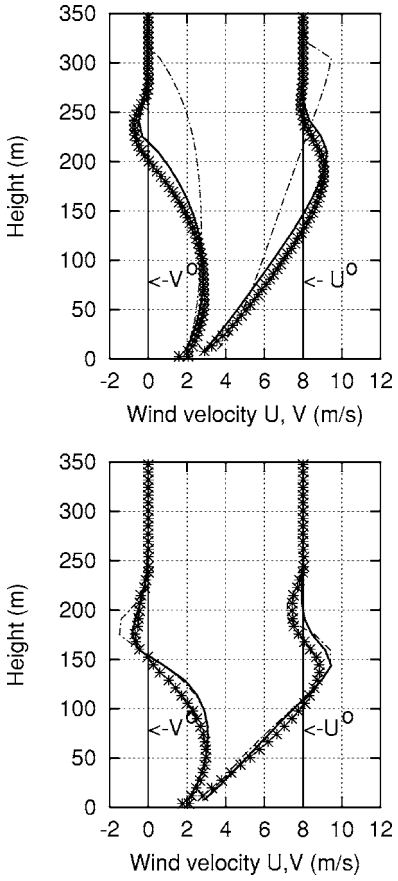

FIG. 12. Vertical profiles of mean horizontal wind components, U and V, simulated with the new and the standard K-ϵ models. The initial profiles are marked as U^0 and V^0, respectively. The order of panels and the description of the lines and asterisks are the same as in Fig. 11.

the prediction accuracy is compromised. Overall, the QNSE-based K-ϵ model has provided quite comparable description of atmospheric SBL in the cases of both moderate and strong stable stratification, simulated with the identical set of constants and with no additional adjustments.

Figure 11 shows profiles of the potential temperature (PT) simulated with the QNSE-based and the standard K-ϵ models as well as with the LES after a 12 real-time hour simulation. The agreement between the present model and LES is good for both cases of moderate and strong stratifications. The standard model strongly overestimates the height of the temperature boundary layer in the case of moderate stratification. The vertical profiles of the horizontal wind components, U and V, are depicted in Fig. 12. The results obtained with the QNSE-based K-ϵ model show good agreement with the LES-computed wind profiles whereas the standard K-ϵ model does not compare well in the case of the moderate stratification.

XIII. DISCUSSION AND CONCLUSIONS

Here we attempted to systematically account for the effect of stable stratification on turbulent flows based upon the hypothesis of quasi-Gaussianity of the velocity and temperature fluctuations combined with the iterative coarse-graining technique. The inherent promise specific to all spectral models—the QNSE model including—is that they start from exact equations in which the effects of pressure, stratification, and incompressibility are solved for rigorously in the canonical equation (19). As a result, it might be expected that the QNSE model accounts for the combined effect of turbulence and waves. In fact, the QNSE model offers a powerful machinery to study wave-turbulence interaction. Among new results are a dispersion relation for internal waves in the presence of turbulence and the critical Froude number/wave number characterizing the threshold of internal wave generation. The wave contribution to the effective viscosities and diffusivities far exceeds in its complexity all other contributions; this is evident from the wave generating poles (110) and the corresponding frequency integrals R^3 and R^4 given by Eqs. (111) and (A1)–(A5) in Appendix A. A combined contribution to mixing and dispersion from turbulence and waves has been emphasized in Refs. 34 and 35 which noted that most of the models available today account for turbulence only, the fact characterized as "a significant shortcoming." The QNSE model is free of this shortcoming.

It was revealed that the Ozmidov wave number plays a profound role in characterization of the effect of stable stratification. It is useful to trace the analogy between the Ozmidov wave number and the transitional wave number, $k_\beta = (\beta^3/\epsilon)^{1/5}$, that characterizes the effect of Rossby waves on

two-dimensional (2D) turbulence on the β plane.[67,68] Recall that k_β was obtained by equating the eddy turnover time scale of turbulence and the period of a linear Rossby wave. The resulting curve, coined "the lazy 8"[69] or "the dumbbell shape"[67] outlined the regions with prevailing influence of 2D turbulence (the exterior of the dumbbell) and Rossby waves (the interior of the dumbbell). A similar surface in the case of stable stratification is described by Eq. (162); it is a torus whose vertical cross section closely resembles the dumbbell shape of the β-plane turbulence. Comparing parameters characterizing those dumbbell shapes, conclude that the Ozmidov wave number k_O is the analog of k_β on the β plane. From the viewpoint of turbulence dynamics, both dumbbell shapes outline the spectral regions of rapid change in flow properties related to strong large-scale anisotropization and the development of slow manifolds along the directions in Fourier space for which wave propagation is prohibited ($k_h=0$ for internal waves and $k_x=0$ for Rossby waves). Further analysis of the analogies between internal and Rossby waves can be found elsewhere.[9,24]

Operating with the horizontal and vertical effective transport coefficients, the QNSE model recognizes the spatial anisotropy induced by stable stratification and reflects energy concentration in the horizontal components at the expense of their vertical counterparts. The practical potential of the QNSE model is in that it is general enough to accommodate the combined effect of internal waves, anisotropy, and diffusion of momentum and heat within one framework and at the same time simple enough to produce results readily available for consumption in LES and RANS models. Note in this regard that this approach required just a single closure relationship in order to connect a modal-statistical derivation with observable physical-space properties; it relates the forcing amplitude and the dissipation rate through the balance between the energy input rate at large scales and the dissipation at small scales.

Note that strictly speaking, the QNSE model predicts the *effective response functions* in the momentum and temperature propagators $G_{\alpha\beta}(\omega,\mathbf{k})$ and $G_T(\omega,\mathbf{k})$ and, through them, the effective viscosities and diffusivities, rather than the *true* eddy viscosities and eddy diffusivities calculated as two-parametric characteristics $\nu(k|k_c)$ and $\kappa(k|k_c)$, where k_c is the wave number separating subgrid and resolvable modes.[70] In 3D flows, except for the cusp behavior at $k\to k_c$, the difference between the effective response functions and the two-parametric characteristics is small and does not significantly affect numerical results. Due to the use of the distant interaction approximation, this cusp cannot be reproduced; however, in principle, it is possible to calculate the two-parametric characteristics from the evolution equations for the second-order moments using the effective response functions.[71] The two-parametric characteristics have not been explored in this study; their analysis should be undertaken in the future research.

Our model predicts that under very strong stable stratification the vertical diffusivity becomes very small while the horizontal diffusivity is enhanced. The same is true for the vertical and horizontal diffusivity of the flow momentum, with the exception that the vertical diffusivity of momentum remains finite due to, supposedly, the effect of internal waves. In connection with this behavior, note that we predict the increase of the turbulent Prandtl number with increasing Ri which is supported by laboratory data and some atmospheric and oceanic observations. Another interesting result produced by the QNSE model is the absence of a critical Richardson number. The model predicts that while there exists a sharp transition in turbulence characteristics for Ri in the range between 0.1 and 1, turbulence survives for the values of Ri in excess of 10. This prediction agrees well with numerous observations in the atmosphere and the ocean[50–53] as well as with the numerical simulations and theoretical considerations.[43,54,72–74]

Although the QNSE model equations for effective viscosities and diffusivities are complicated in the general case of arbitrary stratification, they simplify significantly in the asymptotic case of weak stratification in which analytical expressions can be obtained. These expressions can be used to understand the mechanics of the flow field anisotropization and to calculate various 1D spectra. An important achievement of the QNSE model is the analytical derivation of the new spectrum proportional to $N^2k_3^{-3}$ in addition to the neutral transverse spectrum. The numerical coefficient with this spectrum is in very good agreement with LES.

Turning to the limitations of the presented model, it should be noted that it is designed to operate at moderate stratification. Therefore, the QNSE model should work better at the small scales close to the dissipation range where stratification is weak. With increasing scales, the effect of stratification strengthen. Here, it is assumed that the dressed forcing remains isotropic for any stratification. Although this assumption seems to produce satisfactory results overall, it may become inaccurate under very strong stratification. This problem can be resolved by considering force anisotropization. This is an interesting and important issue which needs to be addressed in future research.

The hypothesis of quasi-Gaussianity is another assumption which may require reevaluation in the future. Here, it appears to yield good results for the second-order moments that produce the essential parameters for the intended application in LES and RANS modeling-effective viscosities and diffusivities. The exploration of the possible effect of non-Gaussianity of higher-order turbulent correlations on the second-order moments remains an important task for the future.

The QNSE model does not consider the direct effect of the mean shear on turbulent fluctuations at the level of the momentum balance. Instead, the mean shear is introduced as the closure assumption at the level of the energy balance. This approach may degrade the accuracy of the model. The mean shear can be included directly in the governing equations; this is yet another issue that needs to be dealt with in future research.

ACKNOWLEDGMENTS

The authors would like to acknowledge stimulating and encouraging discussions with CARTUM scientists throughout the duration of the project. This research has greatly

benefited from discussions with late Joel Ferziger. Lucinda Shih, Jeff Koseff, and Subhas Venayagamoorthy have kindly provided us with their DNS data for comparisons in Sec. XII. Thanks are also extended to Chad Edmisten of the Graphics Department of the College of Marine Science at USF for drawing and processing the figures. Partial support of this research by the ARO Grant No. DAAD19-01-1-0816, the Israel Science Foundation Grant No. 134/03, and NASA grant under Contract No. NAS5-32804 is gratefully appreciated.

APPENDIX A: FREQUENCY INTEGRAL R^4, EQ. (112)

$$R^4 = \int S^4(\Omega,k,k_3,q,q_3)\frac{d\Omega}{2\pi} = -\frac{N^4}{2}\left(\frac{1}{D_1}+\frac{Q_2}{D_2}+\frac{Q_3}{D_3}\right), \tag{A1}$$

where

$$D_1 = N^2P_{33}(\mathbf{q})\omega_q(\omega_{k-q}+\omega_q)[N^2P_{33}(\mathbf{k}-\mathbf{q})+(\omega_{k-q}+\omega_q)\times(\omega_q+\omega_{k-q}^T)], \tag{A2}$$

$$Q_2 = \omega_q^T(\omega_{k-q}+\omega_q^T)^2(\omega_q+\omega_q^T)(\omega_{k-q}^T+\omega_q^T)+N^2(P_{33}(\mathbf{k}-\mathbf{q})\omega_q^T(\omega_{k-q}+\omega_q^T)(\omega_q+\omega_q^T)+P_{33}(\mathbf{q})\{-2\omega_q(\omega_{k-q}+\omega_q)^2-(\omega_{k-q}^2+4\omega_{k-q}\omega_q+2\omega_q^2)\omega_{k-q}^T-2[\omega_{k-q}^2+2\omega_q(\omega_q+\omega_{k-q}^T)+2\omega_{k-q}(2\omega_q+\omega_{k-q}^T)]\omega_q^T-3[2(\omega_{k-q}+\omega_q)+\omega_{k-q}^T]\omega_q^{T^2}-4\omega_q^{T^3}\})+N^4P_{33}(\mathbf{q})\{P_{33}(\mathbf{q})(2\omega_{k-q}+3\omega_q+\omega_{k-q}^T+3\omega_q^T)-P_{33}(\mathbf{k}-\mathbf{q})[\omega_{k-q}+2(\omega_q+\omega_q^T)]\}, \tag{A3}$$

$$D_2 = (\omega_q+\omega_q^T)[N^2P_{33}(\mathbf{q})+\omega_q\omega_q^T][N^2P_{33}(\mathbf{q})+(\omega_{k-q}+\omega_q)(\omega_{k-q}+\omega_q^T)][N^2P_{33}(\mathbf{q})+2\omega_q(\omega_q+\omega_q^T)](N^4[P_{33}(\mathbf{k}-\mathbf{q})-P_{33}(\mathbf{q})]^2+(\omega_{k-q}+\omega_q)(\omega_q+\omega_{k-q}^T)(\omega_{k-q}+\omega_q^T)(\omega_{k-q}^T+\omega_q^T)+N^2\{P_{33}(\mathbf{q})[\omega_{k-q}^2+\omega_{k-q}^T(\omega_q+\omega_{k-q}^T)+(2\omega_q+\omega_{k-q}^T)\omega_q^T+\omega_{k-q}(\omega_q+\omega_q^T)]+P_{33}(\mathbf{k}-\mathbf{q})[\omega_q(\omega_q+\omega_{k-q}^T)+\omega_{k-q}^T\omega_q^T+\omega_q^{T^2}+\omega_{k-q}(\omega_q+2\omega_{k-q}^T+\omega_q^T)]\}), \tag{A4}$$

$$Q_3 = 2(N^4[P_{33}(\mathbf{k}-\mathbf{q})-P_{33}(\mathbf{q})]P_{33}(\mathbf{q})-(\omega_{k-q}+\omega_q^T)^2(\omega_q+\omega_q^T)(\omega_{k-q}^T+\omega_q^T)+N^2\{-P_{33}(\mathbf{k}-\mathbf{q})(\omega_{k-q}+\omega_q^T)(\omega_q+\omega_q^T)+P_{33}(\mathbf{q})\times[\omega_{k-q}^2+2\omega_q(\omega_q+\omega_{k-q}^T)+2(2\omega_q+\omega_{k-q}^T)\omega_q^T+3\omega_q^{T^2}+2\omega_{k-q}(2\omega_q+\omega_{k-q}^T+2\omega_q^T)]\}), \tag{A5}$$

$$D_3 = N^2P_{33}(\mathbf{q})[N^2P_{33}(\mathbf{q})+(\omega_{k-q}+\omega_q)(\omega_{k-q}+\omega_q^T)][N^2P_{33}(\mathbf{q})+2\omega_q(\omega_q+\omega_q^T)](N^4[P_{33}(\mathbf{k}-\mathbf{q})-P_{33}(\mathbf{q})]^2+(\omega_{k-q}+\omega_q)\times(\omega_q+\omega_{k-q}^T)(\omega_{k-q}+\omega_q^T)(\omega_{k-q}^T+\omega_q^T)+N^2\{P_{33}(\mathbf{q})[\omega_{k-q}^2+\omega_{k-q}^T(\omega_q+\omega_{k-q}^T)+(2\omega_q+\omega_{k-q}^T)\omega_q^T+\omega_{k-q}(\omega_q+\omega_q^T)]+P_{33}(\mathbf{k}-\mathbf{q})[\omega_q(\omega_q+\omega_{k-q}^T)+\omega_{k-q}^T\omega_q^T+\omega_q^{T^2}+\omega_{k-q}(\omega_q+2\omega_{k-q}^T+\omega_q^T)]\}). \tag{A5}$$

APPENDIX B: EXPANSION COEFFICIENTS IN EQ. (116)

$$R_0^1 = \frac{1}{4\omega_q^2}, \tag{B1}$$

$$R_z^1 = \frac{\nu_z}{4\omega_q^3}, \tag{B2}$$

$$R_h^1 = \frac{\nu}{4\omega_q^3}, \tag{B3}$$

$$R_0^2 = \frac{-N^2}{4\omega_q^2[N^2P_{33}(\mathbf{q})+2\omega_q(\omega_q+\omega_q^T)]}, \tag{B4}$$

$$R_z^2 = -N^2\{N^2P_{33}(\mathbf{q})(\nu_zq^2-2\omega_q)+4q^2\omega_q[\kappa_z\omega_q+\nu_z(\omega_q+\omega_q^T)]\}/D_2, \tag{B5}$$

$$R_h^2 = -N^2\{2\omega_q(-\{N^2[-1+P_{33}(\mathbf{q})]\}+2\kappa q^2\omega_q)+\nu q^2[N^2P_{33}(\mathbf{q})+4\omega_q(\omega_q+\omega_q^T)]\}/D_2, \tag{B6}$$

$$D_2 = 4q^2\omega_q^3[N^2P_{33}(\mathbf{q})+2\omega_q(\omega_q+\omega_q^T)]^2, \tag{B7}$$

$$R_0^3 = -N^2\frac{N^2P_{33}(\mathbf{q})(\omega_q+\omega_q^T)+\omega_q\omega_q^T(5\omega_q+3\omega_q^T)}{4\omega_q^2(\omega_q+\omega_q^T)[N^2P_{33}(\mathbf{q})+\omega_q\omega_q^T][N^2P_{33}(\mathbf{q})+2\omega_q(\omega_q+\omega_q^T)]}, \tag{B8}$$

$$R_z^3 = -N^2\nu_z[N^4P_{33}(\mathbf{q})^2(\omega_q+\omega_q^T)+8\omega_q^2\omega_q^T(3\omega_q^2+3\omega_q\omega_q^T+\omega_q^{T^2})+N^2P_{33}(\mathbf{q})\omega_q(8\omega_q^2+9\omega_q\omega_q^T+5\omega_q^{T^2})]/D_3, \tag{B9}$$

$$R_h^3 = -N^2\nu\{N^4P_{33}(\mathbf{q})^2(\omega_q+\omega_q^T)+8\omega_q^2\omega_q^T(3\omega_q^2+3\omega_q\omega_q^T+\omega_q^{T^2})+N^2P_{33}(\mathbf{q})\omega_q(8\omega_q^2+9\omega_q\omega_q^T+5\omega_q^{T^2})\}/D_3,$$

$$D_3 = 4\omega_q^3(\omega_q + \omega_q^T)[N^2P_{33}(\mathbf{q}) + \omega_q\omega_q^T][N^2P_{33}(\mathbf{q}) + 2\omega_q(\omega_q + \omega_q^T)]^2, \tag{B10}$$

$$R_0^4 = N^4\frac{N^2P_{33}(\mathbf{q})(2\omega_q^2 + 2\omega_q\omega_q^T + \omega_q^{T^2}) + \omega_q\omega_q^T(4\omega_q^2 + 5\omega_q\omega_q^T + 2\omega_q^{T^2})}{4\omega_q^2(\omega_q + \omega_q^T)^2[N^2P_{33}(\mathbf{q}) + \omega_q\omega_q^T]^2[N^2P_{33}(\mathbf{q}) + 2\omega_q(\omega_q + \omega_q^T)]}, \tag{B11}$$

$$\begin{aligned}R_z^4 = N^4\{&2\nu_z q^2\omega_q^3\omega_q^{T^2}(\omega_q + \omega_q^T)(16\omega_q^3 + 25\omega_q^2\omega_q^T + 18\omega_q\omega_q^{T^2} + 5\omega_q^{T^2}) + N^6P_{33}(\mathbf{q})^3[\nu_z q^2(2\omega_q + \omega_q^T)(\omega_q^2 + \omega_q\omega_q^T + \omega_q^{T^2}) - \omega_q(4\omega_q^3\\ &+ 7\omega_q^2\omega_q^T + 6\omega_q\omega_q^{T^2} + 2\omega_q^{T^3})] + \kappa_z q^2\omega_q^2[N^6P_{33}(\mathbf{q})^3\omega_q + 8\omega_q^2\omega_q^T(\omega_q + \omega_q^T)^4 + N^4P_{33}(\mathbf{q})^2(8\omega_q^3 + 18\omega_q^2\omega_q^T + 13\omega_q\omega_q^{T^2} + 4\omega_q^{T^3})\\ &+ N^2P_{33}(\mathbf{q})\omega_q(\omega_q + \omega_q^T)(4\omega_q^3 + 24\omega_q^2\omega_q^T + 28\omega_q\omega_q^{T^2} + 11\omega_q^{T^3})] + N^4P_{33}(\mathbf{q})^2\omega_q[-\omega_q(4\omega_q^4 + 16\omega_q^3\omega_q^T + 25\omega_q^2\omega_q^{T^2} + 20\omega_q\omega_q^{T^2}\\ &+ 6\omega_q^{T^4}) + \nu_z q^2(12\omega_q^4 + 34\omega_q^3\omega_q^T + 37\omega_q^2\omega_q^{T^2} + 25\omega_q\omega_q^{T^3} + 7\omega_q^{T^4})] + N^2P_{33}(\mathbf{q})\omega_q^2\omega_q^T[-\omega_q(\omega_q + \omega_q^T)(8\omega_q^3 + 16\omega_q^2\omega_q^T\\ &+ 15\omega_q\omega_q^{T^2} + 5\omega_q^{T^3}) + \nu_z q^2(40\omega_q^4 + 102\omega_q^3\omega_q^T + 107\omega_q^2\omega_q^{T^2} + 62\omega_q\omega_q^{T^3} + 15\omega_q^{T^4})]\}/D_4,\end{aligned} \tag{B12}$$

$$\begin{aligned}R_h^4 = N^4\{&\kappa q^2\omega_q^2[N^6P_{33}(\mathbf{q})^3\omega_q + 8\omega_q^2\omega_q^T(\omega_q + \omega_q^T)^4 + N^4P_{33}(\mathbf{q})^2(8\omega_q^3 + 18\omega_q^2\omega_q^T + 13\omega_q\omega_q^{T^2} + 4\omega_q^{T^3}) + N^2P_{33}(\mathbf{q})\omega_q(\omega_q + \omega_q^T)\\ &\times(4\omega_q^3 + 24\omega_q^2\omega_q^T + 28\omega_q\omega_q^{T^2} + 11\omega_q^{T^3})] - N^2\omega_q[-1 + P_{33}(\mathbf{q})][N^4P_{33}(\mathbf{q})^2(4\omega_q^3 + 7\omega_q^2\omega_q^T + 6\omega_q\omega_q^{T^2} + 2\omega_q^{T^3}) + \omega_q^2\omega_q^T(\omega_q\\ &+ \omega_q^T)(8\omega_q^3 + 16\omega_q^2\omega_q^T + 15\omega_q\omega_q^{T^2} + 5\omega_q^{T^3}) + N^2P_{33}(\mathbf{q})\omega_q(4\omega_q^4 + 16\omega_q^3\omega_q^T + 25\omega_q^2\omega_q^{T^2} + 20\omega_q\omega_q^{T^3} + 6\omega_q^{T^4})]\\ &+ \nu q^2[N^6P_{33}(\mathbf{q})^3(2\omega_q + \omega_q^T)(\omega_q^2 + \omega_q\omega_q^T + \omega_q^{T^2}) + 2\omega_q^3\omega_q^{T^2}(\omega_q + \omega_q^T)(16\omega_q^3 + 25\omega_q^2\omega_q^T + 18\omega_q\omega_q^{T^2} + 5\omega_q^{T^3})\\ &+ N^4P_{33}(\mathbf{q})^2\omega_q(12\omega_q^4 + 34\omega_q^3\omega_q^T + 37\omega_q^2\omega_q^{T^2} + 25\omega_q\omega_q^{T^3} + 7\omega_q^{T^4}) + N^2P_{33}(\mathbf{q})\omega_q^2\omega_q^T(40\omega_q^4 + 102\omega_q^3\omega_q^T + 107\omega_q^2\omega_q^{T^2}\\ &+ 62\omega_q\omega_q^{T^3} + 15\omega_q^{T^4})]\}/D_4,\end{aligned}$$

$$D_4 = 4q^2\omega_q^3(\omega_q + \omega_q^T)^3[N^2P_{33}(\mathbf{q}) + \omega_q\omega_q^T]^3[N^2P_{33}(\mathbf{q}) + 2\omega_q(\omega_q + \omega_q^T)]^2. \tag{B13}$$

APPENDIX C: ASYMPTOTIC CASE OF STRONG STRATIFICATION

In the limit of strong stable stratification, $\mathcal{F}\to 0$, the following expressions for Q_1–Q_4 are obtained:

$$\begin{aligned}Q_1 = \frac{1}{64}\Bigg(&\frac{2}{\nu_h\nu_z} + \frac{1}{-\nu_h^2 + \nu_h\nu_z} + \frac{2(\kappa_h + \nu_h)(4\kappa_h + 3\nu_h) + (22\kappa_h + 9\nu_h - 15\kappa_z - 15\nu_z)(\kappa_z + \nu_z)}{(\kappa_h + \nu_h - \kappa_z - \nu_z)^3(\kappa_z + \nu_z)}\\ &- \frac{\kappa_z\{-2(\kappa_h + \nu_h)^2 + (\kappa_z + \nu_z)[9(\kappa_h + \nu_h) + 8\kappa_z + 8\nu_z]\}}{(\kappa_h + \nu_h - \kappa_z - \nu_z)^3(\kappa_z + \nu_z)^2} + \operatorname{arcsinh}\sqrt{-1 + \frac{\nu_h}{\nu_z}}\frac{4\nu_h - 3\nu_z}{[\nu_h(\nu_h - \nu_z)]^{3/2}}\\ &- \operatorname{arcsinh}\sqrt{-1 + \frac{\kappa_h + \nu_h}{\kappa_z + \nu_z}}\sqrt{\frac{\kappa_h + \nu_h}{(\kappa_h + \nu_h - \kappa_z - \nu_z)^5}}\left[\frac{17\kappa_h + 20\nu_h + \kappa_z + \nu_z}{\kappa_h + \nu_h} + \frac{15(\kappa_h - \kappa_z)}{\kappa_h + \nu_h - \kappa_z - \nu_z}\right]\Bigg),\end{aligned} \tag{C1}$$

$$\begin{aligned}Q_2 = \frac{1}{16}&\left[\frac{-20\kappa_h + 2\kappa_z - 21\nu_h}{(\kappa_h + \nu_h)(\kappa_h - \kappa_z + \nu_h - \nu_z)^2} + \frac{\kappa_h + 2\kappa_z + \nu_h}{(\kappa_h + \nu_h)^2(\kappa_h - \kappa_z + \nu_h - \nu_z)} + \frac{2\kappa_z}{(\kappa_h + \nu_h)^2(\kappa_z + \nu_z)} + \frac{15(\kappa_h - \kappa_z)}{(-\kappa_h + \kappa_z - \nu_h + \nu_z)^3}\right]\\ &+ \frac{\operatorname{arcsinh}\sqrt{-1 + [(\kappa_h + \nu_h)/(\kappa_z + \nu_z)]}}{16\sqrt{(\kappa_h + \nu_h)(\kappa_h - \kappa_z + \nu_h - \nu_z)}}\left[\frac{-1}{\kappa_h + \nu_h} + \frac{15(\kappa_h - \kappa_z)(\kappa_h + \nu_h)}{(\kappa_h - \kappa_z + \nu_h - \nu_z)^3} + \frac{3(5\kappa_h + \kappa_z + 7\nu_h)}{(\kappa_h - \kappa_z + \nu_h - \nu_z)^2}\right.\\ &\left.+ \frac{9\kappa_h + 8\nu_h}{(\kappa_h + \nu_h)(-\kappa_h + \kappa_z - \nu_h + \nu_z)}\right],\end{aligned} \tag{C2}$$

$$Q_3 = \frac{\sqrt{1 - (\nu_z/\nu_h)}\operatorname{arcsinh}\sqrt{-1 + (\nu_h/\nu_z)} - \sqrt{1 - [(\kappa_z + \nu_z)/(\kappa_h + \nu_h)]}\operatorname{arcsinh}\sqrt{-1 + [(\kappa_h + \nu_h)/(\kappa_z + \nu_z)]}}{2(\nu_h\kappa_z - \kappa_h\nu_z)}, \tag{C3}$$

$$Q_4 = O(\mathcal{F}^2). \tag{C4}$$

[1] A. E. Gargett, "Ocean turbulence," Annu. Rev. Fluid Mech. **21**, 419 (1989).
[2] G. N. Ivey and J. Imberger, "On the nature of turbulence in a stratified fluid. Part I: The energetics of mixing," J. Phys. Oceanogr. **21**, 650 (1991).
[3] J. Imberger and G. N. Ivey, "On the nature of turbulence in a stratified fluid. Part II: Application to lakes," J. Phys. Oceanogr. **21**, 659 (1991).
[4] F. S. Godeferd and C. Cambon, "Detailed investigation of energy transfers in homogeneous stratified turbulence," Phys. Fluids **6**, 2084 (1994).
[5] C. Cambon and J. F. Scott, "Linear and nonlinear models of anisotropic turbulence," Annu. Rev. Fluid Mech. **31**, 1 (1999).
[6] J. J. Riley and M. P. Lelong, "Fluid motions in the presence of strong stable stratification," Annu. Rev. Fluid Mech. **32**, 613 (2000).
[7] C. Cambon, "Turbulence and vortex structures in rotating and stratified flows," Eur. J. Mech. B/Fluids **20**, 489 (2001).
[8] M. E. Barry, G. N. Ivey, K. B. Winters, and J. Imberger, "Measurements of diapycnal diffusivities in stratified fluids," J. Fluid Mech. **442**, 267 (2001).
[9] L. M. Smith and F. Waleffe, "Generation of slow large scales in forced rotating stratified turbulence," J. Fluid Mech. **451**, 145 (2002).
[10] C. Staquet and J. Sommeria, "Internal gravity waves: From instabilities to turbulence," Annu. Rev. Fluid Mech. **34**, 559 (2002).
[11] H. Hanazaki and J. C. R. Hunt, "Structure of unsteady stably stratified turbulence with mean shear," J. Fluid Mech. **507**, 1 (2004).
[12] S. A. Thorpe, "Recent developments in the study of ocean turbulence," Annu. Rev. Earth Planet Sci. **32**, 91 (2004).
[13] *Marine Turbulence—Theories, Observations and Models*, edited by H. Z. Baumert, J. Simpson, and J. Sundermann (Cambridge University Press, Cambridge, 2005).
[14] S. A. Orszag, in *Les Houches Summer School in Physics*, edited by R. Balian and J.-L. Peabe (Gordon and Breach, New York, 1977), p. 237.
[15] W. D. McComb, *The Physics of Fluid Turbulence* (Oxford University Press, New York, 1991).
[16] R. H. Kraichnan, "An interpretation of the Yakhot-Orszag turbulence theory," Phys. Fluids **30**, 2400 (1987).
[17] D. Forster, D. R. Nelson, and M. J. Stephen, "Large distance and long-time properties of a randomly stirred fluid," Phys. Rev. A **16**, 732 (1977).
[18] V. Yakhot and S. A. Orszag, "Renormalization group analysis of turbulence. I. Basic theory," J. Sci. Comput. **1**, 3 (1986).
[19] L. M. Smith and S. L. Woodruff, "Renormalization-group analysis of turbulence," Annu. Rev. Fluid Mech. **30**, 275 (1998).
[20] S. Sukoriansky, B. Galperin, and I. Staroselsky, "Cross-terms and ϵ-expansion in RNG theory of turbulence," Fluid Dyn. Res. **33**, 319 (2003).
[21] M. Lesieur, *Turbulence in Fluids*, 3rd ed. (Kluwer, Dordrecht, 1997).
[22] C. Staquet and F. S. Godeferd, "Statistical modelling and direct numerical simulations of decaying stably stratified turbulence. Part 1. Flow energetics," J. Fluid Mech. **360**, 295 (1998).
[23] F. S. Godeferd and C. Staquet, "Statistical modelling and direct numerical simulations of decaying stably stratified turbulence. Part 2. Large-scale and small-scale anisotropy," J. Fluid Mech. **486**, 115 (2003).
[24] C. Cambon, R. Rubinstein, and F. S. Godeferd, "Advances in wave turbulence: rapidly rotating flows," New J. Phys. **6**, 73 (2004).
[25] W. D. McComb and C. Johnston, "Conditional mode elimination and scale-invariant dissipation in isotropic turbulence," Physica A **292**, 346 (2001).
[26] R. H. Kraichnan, "Inertial-range transfer in two- and three-dimensional turbulence," J. Fluid Mech. **47**, 525 (1971).
[27] V. M. Canuto and M. S. Dubovikov, "Dynamical model for turbulence: I. General formalism," Phys. Fluids **8**, 571 (1996).
[28] I. M. Gel'fand and G. E. Shilov, *Generalized Functions*, Properties and Operations Vol. 1 (Harcourt Brace, New York, 1977).
[29] S. A. Orszag, I. Staroselsky, and V. Yakhot, in *Large Eddy Simulation of Complex Engineering and Geophysical Flows*, edited by B. Galperin and S. A. Orszag (Cambridge University Press, Cambridge, 1993), pp. 55–78.
[30] V. M. Tsarenko, and A. M. Yaglom, in *Studies in Turbulence*, edited by T. B. Gatski, S. Sarkar, and C. G. Speziale (Springer, Berlin, 1992), pp. 39–59.
[31] W. P. Dannevik, V. Yakhot, and S. A. Orszag, "Analytical theories of turbulence and the ϵ-expansion," Phys. Fluids **30**, 2021 (1987).
[32] K. Sreenivasan, "On the universality of the Kolmogorov constant," Phys. Fluids **7**, 2778 (1995).
[33] L. D. Landau and E. M. Lifshitz, *Fluid Mechanics*, 2nd ed. (Pergamon, Oxford, 1993).
[34] E. A. D'Asaro and R.-C. Lien, "Lagrangian measurements of waves and turbulence in stratified flows," J. Phys. Oceanogr. **30**, 641 (2000).
[35] E. A. D'Asaro and R.-C. Lien, "The wave-turbulence transition for stratified flows," J. Phys. Oceanogr. **30**, 1669 (2000).
[36] A. S. Monin and A. M. Yaglom, *Statistical Fluid Mechanics* (MIT Press, Cambridge, MA, 1975).
[37] J. L. Lumley, "The spectrum of nearly inertial turbulence in a stable stratified fluid," J. Atmos. Sci. **21**, 99 (1964).
[38] O. M. Phillips, *The Dynamics of the Upper Ocean*, 2nd ed. (Cambridge University Press, Cambridge, 1977).
[39] G. Holloway, "Considerations on the theory of temperature spectra in stably stratified turbulence," J. Phys. Oceanogr. **16**, 2179 (1986).
[40] A. E. Gargett, P. J. Hendricks, T. B. Sanford, T. R. Osborn, and A. J. Williams III, "A composite spectrum of vertical shear in the upper ocean," J. Phys. Oceanogr. **11**, 1258 (1981).
[41] G. F. Carnevale, M. Briscolini, and P. Orlandi, "Buoyancy- to inertial-range transition in forced stratified turbulence," J. Fluid Mech. **427**, 205 (2001).
[42] S. H. Derbyshire and J. C. R. Hunt, in *Waves and Turbulence in Stably Stratified Flows*, edited by S. D. Mobbs and J. C. King (Clarendon, Oxford, 1993), pp. 23-59.
[43] E. Lindborg, "The effect of rotation on the mesoscale energy cascade in the free atmosphere," Geophys. Res. Lett. **32**, L01809 (2005).
[44] L. H. Shih, J. R. Koseff, J. H. Ferziger, and C. R. Rehmann, "Scaling and parameterization of stratified homogeneous turbulent shear flow," J. Fluid Mech. **412**, 1 (2000).
[45] S. K. Venayagamoorthy, J. R. Koseff, J. H. Ferziger, and L. H. Shih, *CTR Annual Research Briefs* (NASA, Ames, Palo Alto, CA, 2003).
[46] G. L. Mellor and T. Yamada, "Development of a turbulence closure model for geophysical fluid problems," Rev. Geophys. Space Phys. **20**, 851 (1982).
[47] J. W. Miles, "On the stability of heterogeneous shear flows," J. Fluid Mech. **10**, 496 (1961).
[48] L. N. Howard, "Note on a paper of John W. Miles," J. Fluid Mech. **10**, 509 (1961).
[49] H. D. Abarbanel, D. D. Holm, J. E. Marsden, and T. Ratiu, "Richardson number criterion for the nonlinear stability of three-dimensional stratified flow," Phys. Rev. Lett. **52**, 2352 (1984).
[50] E. J. Strang and H. J. S. Fernando, "Vertical mixing and transports through a stratified shear layer," J. Phys. Oceanogr. **31**, 2026 (2001).
[51] P. Monti, H. J. S. Fernando, M. Princevac, W. C. Chan, T. A. Kowalewski, and E. R. Pardyjak, "Observations of flow and turbulence in the nocturnal boundary layer over a slope," J. Atmos. Sci. **59**, 2513 (2002).
[52] A. Mahalov, B. Nicolaenko, K. L. Tse, and B. Joseph, "Eddy mixing in jet-stream turbulence under stronger stratification," Geophys. Res. Lett. **31**, L23111 (2004).
[53] S. A. Mack and H. C. Schoeberlein, "Richardson number and ocean mixing: Towed chain observations," J. Phys. Oceanogr. **34**, 736 (2004).
[54] B. Joseph, A. Mahalov, B. Nicolaenko, and K. L. Tse, "Variability of turbulence and its outer scales in a model tropopause jet," J. Atmos. Sci. **61**, 621 (2004).
[55] F. Einaudi and J. J. Finnigan, "Wave-turbulence dynamics in the stably stratified boundary layer," J. Atmos. Sci. **50**, 1841 (1993).
[56] J. J. Finnigan, "A note on wave-turbulence interaction and the possibility of scaling the very stable boundary layer," Boundary-Layer Meteorol. **90**, 529 (1999).
[57] W. G. Large, J. C. McWilliams, and S. C. Doney, "Oceanic vertical mixing: A review and a model with nonlocal boundary layer parameterization," Rev. Geophys. **32**, 363 (1994).
[58] H. Peters, M. C. Gregg, and J. M. Toole, "On the parameterization of equatorial turbulence," J. Geophys. Res. **93**, 1199 (1988).
[59] M. Cane, in *Large Eddy Simulation of Complex Engineering and Geophysical Flows*, edited by B. Galperin and S. A. Orszag (Cambridge University Press, Cambridge, 1993), pp. 489–509.
[60] L. H. Kantha and C. A. Clayson, "An improved mixed-layer model for geophysical applications," J. Geophys. Res. **99**, 25235 (1994).
[61] J. Kondo, O. Kanechika, and N. Yasuda, "Heat and momentum transfer under strong stability in the atmospheric surface layer," J. Atmos. Sci. **35**, 1012 (1978).
[62] S. Sukoriansky, B. Galperin, and V. Perov, "Application of a new spectral theory of stably stratified turbulence to atmospheric boundary layers over sea ice," Boundary-Layer Meteorol. (in press).
[63] B. Kosovic and J. A. Curry, "A large eddy simulation study of a quasi-steady, stably stratified atmospheric boundary layer," J. Atmos. Sci. **57**,

1052 (2000).
[64] V. Perov and S. Gollvik, "A 1-D test of a non-local K-ϵ boundary layer scheme for a NWP model resolution," HIRLAM Technical Report 25 (1996).
[65] V. Perov, S. Zilitinkevich, and K.-I. Ivarsson, "Implementation of new parameterisation of the surface turbulent fluxes for stable stratification in the 3-D HIRLAM," HIRLAM Newsletter **38**, 88 (2001).
[66] H. Detering and D. Etling, "Application of the $E-\epsilon$ model to the atmospheric boundary layer," Boundary-Layer Meteorol. **33**, 113 (1985).
[67] G. K. Vallis and M. E. Maltrud, "Generation of mean flows and jets on a beta plane and over topography," J. Phys. Oceanogr. **23**, 1346 (1993).
[68] A. Chekhlov, S. A. Orszag, S. Sukoriansky, B. Galperin, and I. Staroselsky, "The effect of small-scale forcing on large-scale structures in two-dimensional flows," Physica D **98**, 321 (1996).
[69] G. Holloway, in *Predictability of Fluid Motions*, edited by G. Holloway and B. J. West (American Institute of Physics, New York, 1984), pp. 593–599.
[70] R. H. Kraichnan, "Eddy viscosity in two and three dimensions," J. Atmos. Sci. **33**, 1521 (1976).
[71] A. Chekhlov, S. A. Orszag, S. Sukoriansky, B. Galperin, and I. Staroselsky, "Direct numerical simulation tests of eddy viscosity in two dimensions," Phys. Fluids **6**, 2548 (1994).
[72] A. Babin, A. Mahalov, B. Nicolaenko, and Y. Zhou, "On the asymptotic regimes and the strongly stratified limit of rotating Boussinesq equations," Theor. Comput. Fluid Dyn. **9**, 223 (1997).
[73] S. H. Derbyshire, "Stable boundary-layer modelling: Established approaches and beyond," Boundary-Layer Meteorol. **90**, 423 (1999).
[74] M. J. Otte and J. C. Wyngaard, "Stably stratified intefacial-layer turbulence from large-eddy simulation," J. Atmos. Sci. **58**, 3424 (2001).